Tectonics®

RESEARCH ARTICLE
10.1029/2021TC007164

Deformation and Material Transfer in a Fossil Subduction Channel: Evidence From the Island of Elba (Italy)

Samuele Papeschi[1], Paola Vannucchi[2], Takehiro Hirose[1], and Keishi Okazaki[1,3]

[1]Kochi Institute for Core Sample Research (X-Star), Japan Agency for Marine-Earth Science and Technology (JAMSTEC), Nankoku, Japan, [2]Dipartimento di Scienze della Terra, Università di Firenze, Firenze, Italy, [3]Earth and Planetary Systems Science Program, Graduate School of Advanced Science and Engineering, Hiroshima University, Higashi-Hiroshima, Hiroshima, Japan

Key Points:

- An exhumed plate boundary zone is preserved at the contact between oceanic and continental units in the inner Northern Apennines
- Subduction caused the coupling of sediments with upper plate serpentinites, producing tectonic mélanges and duplexes
- Episodes of tectonic erosion and underplating are proposed as viable mechanisms to explain the architecture of the subduction channel

Correspondence to:
S. Papeschi,
s.papeschi@gmail.com

Citation:
Papeschi, S., Vannucchi, P., Hirose, T., & Okazaki, K. (2022). Deformation and material transfer in a fossil subduction channel: Evidence from the Island of Elba (Italy). *Tectonics*, *41*, e2021TC007164. https://doi.org/10.1029/2021TC007164

Received 4 DEC 2021
Accepted 19 JUN 2022

Author Contributions:

Conceptualization: Samuele Papeschi, Paola Vannucchi
Data curation: Samuele Papeschi
Formal analysis: Samuele Papeschi, Paola Vannucchi
Funding acquisition: Takehiro Hirose
Investigation: Samuele Papeschi, Paola Vannucchi
Methodology: Samuele Papeschi
Project Administration: Takehiro Hirose
Resources: Samuele Papeschi, Paola Vannucchi, Takehiro Hirose
Software: Samuele Papeschi
Supervision: Paola Vannucchi, Takehiro Hirose, Keishi Okazaki
Validation: Samuele Papeschi, Paola Vannucchi
Visualization: Samuele Papeschi
Writing – original draft: Samuele Papeschi
Writing – review & editing: Samuele Papeschi, Paola Vannucchi, Takehiro Hirose, Keishi Okazaki

Abstract We document an exhumed plate boundary shear zone—a subduction channel—developed at the contact between a fossil Cretaceous-Eocene accretionary prism (Ligurian Units) and the underlying continent-derived nappes of the Northern Apennines. The subduction channel, referred to as the Norsi-Cavo Complex (NCC), is continuously exposed for ~10 km along strike on the island of Elba. The NCC consists of oceanic sediments and serpentinites, coupled at the base of the prism. In its northernmost exposures the NCC crops out as a serpentinite mélange with blocks of sedimentary rocks. There, evidence of pervasive fluid-rock interaction is present. We interpret this mélange as the result of material transfer from the upper plate to the subduction channel through tectonic erosion at the base of the prism. The southern part of the NCC preserves a series of tectonic slices of shales and limestones (Palombini shales) coupled with ultramafic rocks through serpentinite shear zones containing lenses of massive serpentinites, mafic rocks, and sediments. Since sedimentary slices preserve the same structures of the overlying Ligurian Units, produced by accretionary prism deformation, we interpret this complex as the result of material transfer from the prism to the subduction channel and its subsequent underplating at the base of the prism. Based on our interpretation, the NCC fossil subduction channel formed during E-verging deformation over the W-directed subduction of the Ligurian Ocean during the early development stages of the Apennines. This deformation terminated when the continental margin entered the subduction.

Plain Language Summary Subduction is the process by which the ocean floor disappears, pushed by plate tectonics to sink under a continental margin of another oceanic plate. Subduction produces the most destructive earthquakes on Earth and large submerged chains of oceanic rocks called accretionary prisms. Here we describe a belt of deformed rocks on the island of Elba Italy, which we interpret as the emerged analog of a subduction zone that formed between 145 and 35 million years ago in the Northern Apennines of Italy. Subduction produced a complex of intensely deformed rocks, derived from an extinct ocean, underneath a pile of ocean-derived material—called the Ligurian Units. This complex, which we call Norsi-Cavo Complex, witness the crushing of rocks in the subduction zone, which were folded, fragmented, and mixed up in an environment rich in fluids. Deformation structures show that the rocks were transported toward the East, a direction consistent with that of the subduction system. We also propose that during subduction, material was scraped away from the accretionary prism and brought at depth in the subduction zone. At about 35 million years ago, the margin of a continent (Adria) entered subduction and sealed this fossil subduction zone.

1. Introduction

At convergent plate boundaries strain is distributed within a shear zone of variable thickness that forms at the contact between the subducting plate and the overriding plate and which is often referred to as the subduction channel (Cloos & Shreve, 1988a, 1998b; Clift & Vannucchi, 2004; Gerya et al., 2002; Shreve & Cloos, 1986; Vannucchi et al., 2012a; Zhang, 2020). The subduction channel, which may reach 2–3 km in thickness, consists of a rheologically complex mixture of sediments, variably saturated by fluids, and blocks or lenses of different lithologies offscraped from the undergoing slab or eroded from the overlying plate (Abers et al., 2006; Agard et al., 2018; Bebout & Penniston-Dorland, 2016; Collot et al., 2011). At deep crustal levels (>30–35 km), serpentinites from the mantle wedge are thought to become an essential component of the subduction channel (Blanco-Quintero et al., 2011; Federico et al., 2007; Guillot et al., 2004; Schwartz et al., 2001; Wakabayashi, 2019). Understanding the mechanical behavior of the subduction channel is a central objective in the geosciences, because this structure releases some of the greatest magnitude earthquakes on Earth and produces a wide range of geodetically and

seismically detectable slow earthquakes, characterized by slow creep and low- to very low-frequency seismic signals (Ide et al., 2007; Obara, 2002; Obara & Kato, 2016; Rogers & Dragert, 2003; Schwartz & Rokosky, 2007; Shelly et al., 2006). Moreover, the processes active in the subduction channel are responsible for several geological phenomena that are only partially understood, such as the movement of fluids and fluid-rock interaction in subduction zones (Bebout & Penniston-Dorland, 2016 and references therein; Taetz et al., 2018), the recycling of crustal material and fluids into the mantle (Ayers, 1998; Clift et al., 2009; Okamoto et al., 2021; Peacock, 1990), and the exhumation of deep-seated metamorphic rocks (Agard et al., 2018; Maruyama et al., 1996; Guillot et al., 2009; and references therein, Agard et al., 2009; Plunder et al., 2015; Ring et al., 2020). All these processes coexist and interact in the subduction channel, influencing the short- and long-term behavior of subduction zones (e.g., Audet & Bürgmann, 2014; Fisher & Brantley, 2014; Locatelli et al., 2019).

Geophysical imaging and geodetic data provided a wealth of information about presently active subduction channels, especially at shallow structural levels (<15–20 km) (Aoki et al., 1982; Bangs et al., 2009; Gao & Wang, 2017; Kimura et al., 2010; Peng & Gonberg, 2010; Sage et al., 2006). For example, Collot et al. (2011) investigated the subduction channel off the Ecuador coast constraining its thickness to 0.6–1.1 km and documenting its internal structure, characterized by coexisting normal faults, thrusts, and duplex structures developing in response to the mechanical properties of the subducting material and the presence of asperities in the subducting slab. In the same area, velocity models revealed that the subduction channel sediments are much more saturated in fluids than the underlying slab and the overlying accretionary prism, suggesting that fluid drainage occurs predominantly along the subduction interface (Calahorrano et al., 2008).

Unfortunately, our understanding of the subduction channel is limited by the resolution of the geophysical techniques and the impossibility to access the internal structure of presently active subduction zones. Geological investigations of exhumed subduction complexes are fundamental to bridge the scale gap between the geophysical record and geologic materials and obtain direct mechanical estimates from subducted rocks (e.g., Angiboust et al., 2014, 2015; Bachmann, Oncken, et al., 2009; Fagereng, 2011; Kotowski & Behr, 2019; Meneghini & Moore, 2007; Rowe et al., 2011, 2013; Ujiie et al., 2007; Vannucchi et al., 2008). However, the destructive nature of subduction limits the availability of subducted rocks in present orogenic setting. Indeed, some of the most complete inland exposures of ophiolite sequences derive mostly from fragments of back-arc crust that was obducted onto continental margins (e.g., Pearce et al., 1981; Searle & Cox, 1999). The fragments of ocean-derived rocks preserved in the suture zone of orogenic belts, and that witnessed the subduction process before continental collision, are often strongly overprinted by orogenic deformation, metamorphism, and exhumation processes. This limits our possibilities to investigate outcrops preserving fabrics attained during subduction.

In this sense, the Northern Apennines of Italy offer one of the best-preserved exposures of a fossil accretionary prism that registered Alpine subduction before being thrust on top of a continental margin, during the subsequent orogenic deformation (e.g., Boccaletti et al., 1971; Treves, 1984). Indeed, recent studies have shown that the base of the oceanic units in the external area of the belt, deformed in a late Cretaceous to Eocene accretionary prism (preserved in the so called Ligurian Units), exposes a full section through a fossil erosive subduction channel (Vannucchi et al., 2008).

In the present study, we investigated in detail a shear zone, namely the Norsi-Cavo Complex, NCC, that is present at base of the Ligurian Units on the island of Elba (inner Northern Apennines). We interpret the NCC as a fossil and now exhumed subduction channel developed in the hinterland of the orogenic belt. This subduction channel consists of oceanic sediments, mafic and ultramafic material organized in intensely deformed—yet still coherent—tectonic slices, and disrupted, tectonic mélanges. Here we describe in detail two different key sites that show structures that can be referred respectively to processes linked to tectonic erosion from the base of the prism, and underplating of material from the subduction channel to the overlying prism.

2. Geological Background

2.1. Geology of the Northern Apennines

The Northern Apennines (Figure 1) are an ENE-verging orogenic belt produced by the closure of the Alpine Tethys Ocean and the subsequent involvement of the Adria continental margin in a westward subduction zone underneath the European margin. Subduction was accompanied by eastward slab rollback which is linked to the opening of the Tyrrhenian back-arc basin (Boccaletti et al., 1971; Coward & Dietrich, 1989; Elter, 1975a; Faccenna et al., 1996, 2001; Kligfield, 1979; Malinverno & Ryan, 1986; Molli et al., 2018; Patacca et al., 1990;

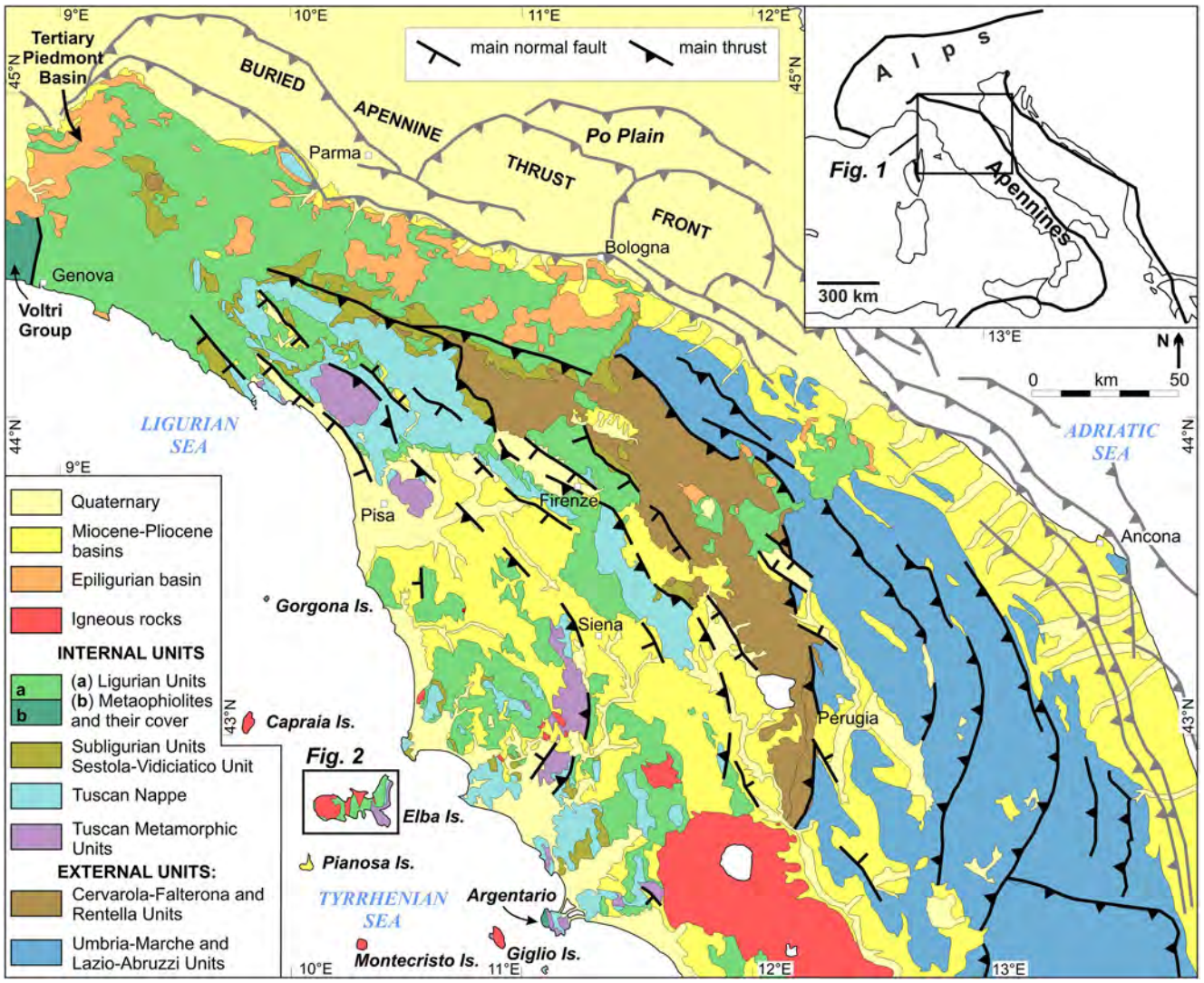

Figure 1. Geologic sketch map of the Northern Apennines (Italy), highlighting the main nappes and the tectonic lineaments of the belt. Based on Conti et al. (2020) and Bonini et al. (2014).

Treves, 1984). The Alpine Tethys, also known as Ligure-Piemontese Ocean, was a Jurassic slow-spreading ocean, with peridotites and gabbros tectonically exposed on the seafloor, locally overlain by basalts or covered by Tethyan sedimentary sequences (Abbate et al., 1986; Elter, 1975b; Elter et al., 1966; Lagabrielle & Cannat, 1990; Le Breton et al., 2021; Marroni & Pandolfi, 2007). This ocean closed during the Cretaceous-Eocene producing the W-vergent Alpine belt, exposed in Alpine Corsica to the west, and the E-vergent Apennine belt which extends from Liguria and crosses the entire Italian peninsula from NNW to SSE. The two belts are interpreted as the result of two subduction systems with opposite vergence (eastward and westward): some models argue for subduction polarity reversal during the formation of the Alps and the Apennines (e.g., Molli, 2008; Marroni et al., 2017), while others propose an along-strike change from an E-dipping to a W-dipping subduction system present since the onset of convergence in the Cretaceous (e.g., Argnani, 2012; Vignaroli et al., 2008). In the Apennines side, the Cretaceous-Eocene oceanic subduction produced an accretionary prism of ocean-derived nappes, collectively known as the Ligurian Units (Figure 1; Elter & Marroni, 1991; Marroni & Pandolfi, 1996; Marroni et al., 2010; Principi & Treves, 1984; Treves, 1984). From the Oligocene onward, the Ligurian Units were thrust onto the Adria continental margin and currently occupy the highest structural level of the Apennine nappe pile (Figure 1; Conti et al., 2020 and references therein). Sandwiched between the Ligurian and the continental Adria-derived units, the Subligurian Units preserve the earliest foredeep deposits of the Apennines (Catanzariti et al., 2003;

Elter et al., 1964, 1999) and tectonic mélanges produced by tectonic erosion in the subduction channel (Remitti et al., 2011; Vannucchi et al., 2008; Vannucchi, Remitti et al., 2012). As the thrust front propagated toward the ENE, the underthrust Adria-derived units (the Tuscan Units and various external units) were incorporated as nappes in the orogenic wedge. These units are capped by foredeep deposits progressively younger toward the external ENE areas of the belt (Boccaletti et al., 1990; Ricci Lucchi, 1986). In the Northern Apennines hinterland, the Tuscan Units (Figure 1) consist of the Tuscan Nappe, characterized by anchizone-facies passive-margin sequences (e.g., Baldacci et al., 1967; Ciarapica & Passeri, 1994; Cerrina-Feroni et al., 1983), and the Tuscan Metamorphic Units, that involve a series of thick-skinned nappes that registered subduction-related greenschist- to blueschist-facies metamorphism (Franceschelli et al., 1986; Papeschi et al., 2022; Rossetti et al., 2002; Theye et al., 1997 and references therein). Wedge-top basins (i.e., Epiligurian Basin; Figure 1) and intermontane basins cover the orogen and show that the belt evolved primarily as an underwater wedge until emersion in the Pliocene (Bonini et al., 2014 and references therein). Extrusive and intrusive rocks of predominant granitic composition were emplaced during the Miocene–Quaternary in the hinterland of the belt (Figure 1; e.g., Serri et al., 1993). The Miocene–Quaternary evolution of the belt is classically interpreted as a consequence of the Adriatic slab rollback with propagation of the thrust front to the east followed by extension and the onset of magmatism in the rear of the wedge (Faccenna et al., 2014; Le Breton et al., 2017; Malinverno & Ryan, 1986). In this framework, the extension in the Northern Tyrrhenian area has been interpreted as continuous from the Miocene to present (e.g., Bartole, 1995; Jolivet et al., 1998; Mauffret et al., 1999; Moeller et al., 2013, 2014) or as discontinuous with a pulse of late Miocene contraction that interrupted the extensional tectonic regime (e.g., Bonini et al., 2014; Molli et al., 2018; Viola et al., 2018). For more details on these different views, the reader is referred to Jolivet et al. (2021) and Ryan et al. (2021).

To summarize, the Ligurian Units, accreted during oceanic subduction, are preserved at the top of the nappe pile and have a very low- metamorphic grade (diagenesis–anchizone). Only the ophiolitic units on the island of Gorgona and on the Argentario Promontory show a blueschist-facies imprint (Decandia & Lazzarotto, 1980; Rossetti et al., 2001, Figure 1).

2.2. Geology of the Island of Elba

Located in the middle of the Tyrrhenian Sea, the Island of Elba represents the innermost exposure of the Northern Apennines hinterland (Figure 1). The Elba nappe stack (map in Figure 2 and detailed cross sections in Figure 3) resulted from Cretaceous-Eocene oceanic subduction, which involved the Ligurian Units (Figure 2; see below), and the subsequent Oligocene–early Miocene collision which caused underthrusting, exhumation, and stacking of a series of Adria continental units underneath the Ligurian Units (Keller & Pialli, 1990; Massa et al., 2017; Pertusati et al., 1993; Ryan et al., 2021). This early Miocene collision event is responsible for the current architecture of the nappe stack, characterized by overall N-S striking and W-dipping thrusts and foliations (Figures 3a and 3b) and general ENE-vergence (Figures 2 and 3; Barberi et al., 1969; Keller & Coward, 1996; Massa et al., 2017; Perrin, 1975 and references therein). The continental units, stacked during the Oligocene–early Miocene, comprise from top to bottom (Figure 3a): (a) the anchizone-facies Tuscan Nappe (illite crystallinity/$\Delta 2\theta = 0.25 - 0.39$; Pandeli et al., 2001), (b) the greenschist-facies Rio Marina Unit (Deschamps et al., 1983), and the amphibolite-facies (c) Ortano and (d) Calamita Units (Musumeci et al., 2011; Musumeci & Vaselli, 2012; Papeschi & Musumeci, 2019; Papeschi et al., 2017, 2018). Amphibolite-facies metamorphism—at $P < 0.2$ GPa and $T \leq 650$°C–700°C—developed during the late Miocene emplacement of the igneous rocks in the upper crust which overprinted the structural and metamorphic fabric of the Ortano and Calamita Units (Duranti et al., 1992; Papeschi et al., 2019). Nevertheless, parts of the Ortano Unit (Figures 2 and 3a) still preserve early Miocene (19–20 Ma) blueschist-facies parageneses ($P \sim 1.5$–1.8 GPa at $T = 320$°C–370°C; Papeschi et al., 2020) and blueschist-greenschist shear zones that accommodated top-to-W syn-orogenic extrusion within the E-vergent nappe stack at 19–20 Ma (Figure 3a; Ryan et al., 2021), producing a normal metamorphic gradient with high pressure units located at the bottom of the nappe stack (Figure 3a). Top-to-W shear zones, likely originally present at the contacts between different nappes, were subsequently reactivated as top-to-E thrusts during the middle-late Miocene tectonics of Elba (Massa et al., 2017; Musumeci & Vaselli, 2012; Ryan et al., 2021).

The Miocene to present tectonics of Elba was marked by the opening of the Northern Tyrrhenian Sea and the emplacement of late Miocene intrusive rocks (e.g., Barboni et al., 2015; Dini et al., 2002; Gagnevin et al., 2011) at high crustal level ($P < 0.2$ GPa; Rossetti et al., 2007; Papeschi et al., 2019). Plutons have been classically

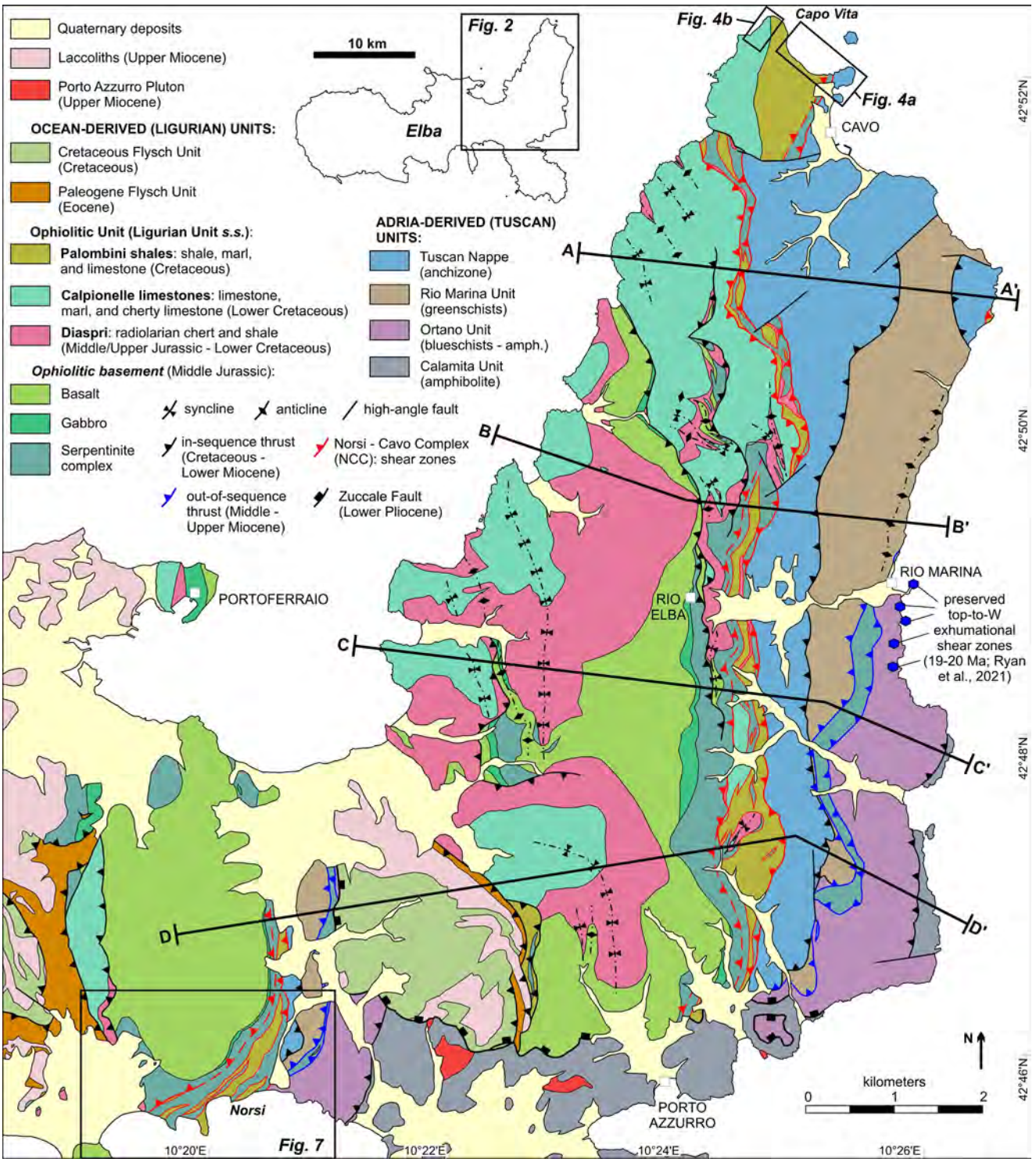

Figure 2. Geologic sketch map of NE Elba, showing the main units and tectonic structures of the area. Formations and lithodemes are shown only for the Ophiolitic Unit of the Ligurian Units. All other units of the nappe stack appear undifferentiated in the map. Black lines, labeled from A to D highlight the location of cross-sections, shown in Figure 3b. Based on Barberi et al. (1967), Perrin (1975), Principi et al. (2015), and Massa et al. (2017). The location of top-to-W shear zones, related to exhumation of the blueschist-facies Ortano Unit and described by Ryan et al. (2021), is highlighted by blue hexagons.

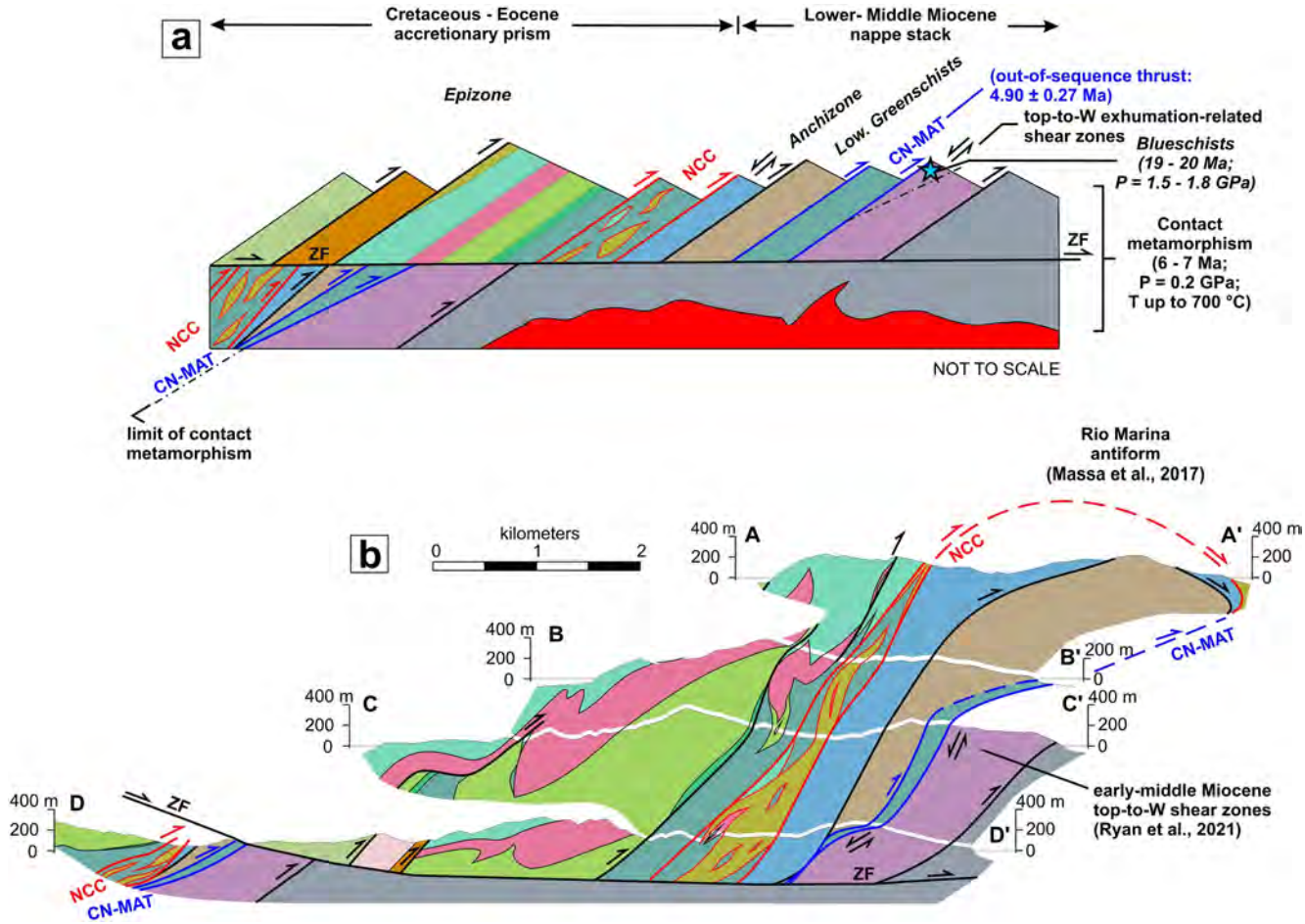

Figure 3. Cross-sections through Eastern Elba. (a) Block diagram showing the present-day relations between tectonic units and magmatic intrusions (laccoliths not shown) (based on an unpublished, historical geologic sketch by Livio Trevisan, 1951–1953). (b) Composite geological cross-sections (a–d) though Eastern Elba (location in Figure 2). Note the presence of a middle-late Miocene antiform (Rio Marina antiform; Massa et al., 2017), refolding the NCC. See text for further details. NCC: Norsi-Cavo Complex; CN–MAT: Capo Norsi-Monte Arco Thrust; ZF: Zuccale Fault. Data: 4.90 ± 0.27 Ma K/Ar age (Viola et al., 2018); 19–20 Ma Ar/Ar age (Ryan et al., 2021 and references therein); metamorphic constraints: Papeschi et al. (2019, 2020) and references therein.

interpreted as emplaced in an extensional setting along low-angle normal faults (e.g., Jolivet et al., 1998, 2021; Keller & Coward, 1996; Pertusati et al., 1993; Smith et al., 2011). Recent studies argue that pluton emplacement in the late Miocene was coeval with out-of-sequence thrusting instead (Musumeci & Vaselli, 2012; Papeschi et al., 2017, 2021; Viola et al., 2018). Despite these different interpretations (see Ryan et al., 2021 for a thorough discussion), the latest faulting event that affected the nappe pile is represented by the Zuccale Fault (ZF; Collettini & Holdsworth, 2004; Musumeci et al., 2015; Smith et al., 2011), a subhorizontal structure (Figure 3) that was recently dated to the early Pliocene (Viola et al., 2018) and that is either interpreted as a low-angle normal fault or a thrust. In this context, the architecture of the Elba nappe stack appears to have been only marginally reworked: recent geophysical studies, indeed, do not document large-scale low-angle normal faults in the Northern Tyrrhenian Sea, suggesting extension localized mostly on high-angle structures (Moeller et al., 2013, 2014), while most of the proposed out-of-sequence thrusts appear localized on the margins of or within contact aureoles (e.g., Papeschi et al., 2017). The only significant reworking of the nappe stack appears to be a middle-late Miocene out-of-sequence thrust, dated at 4.90 ± 0.27 Ma by K/Ar fault gouge dating (Viola et al., 2018) associated with an antiform of nappes in eastern Elba (the Capo Norsi-Monte Arco Thrust; CN-MAT), which brought the pack of continental units on top of a slice of Ligurian-derived serpentinite (Massa et al., 2017), in turn juxtaposed to contact aureole rocks (Figures 2 and 3).

The Ligurian Units on top of the wedge largely escaped the Miocene-present tectonics and their architecture is widely regarded as related mostly to the oceanic subduction stage (Bortolotti et al., 2001; Keller & Pialli, 1990;

Perrin, 1975; Principi et al., 2015). The Ligurian Units on Elba comprise, from top to bottom, (a) Cretaceous terrigenous and carbonatic flysch deposits (Cretaceous Flysch Unit), (b) Paleogene carbonatic-terrigenous flysch (Paleogene Flysch Unit), and (c) the Ophiolitic Unit, a tectonized sequence of Jurassic ophiolites and their Jurassic-Cretaceous sedimentary cover (Figure 2; Barberi et al., 1969; Bortolotti et al., 2001; Perrin, 1975; Reutter & Spohn, 1982; Nirta et al., 2005; referred to as Ligurian Unit in Massa et al., 2017). The ophiolitic basement comprises a sequence of N-MORB pillow basalt, overlying rare and discontinuous lenses of gabbro and a thick serpentinite complex consisting of serpentinites derived from peridotites with harzburgite to lherzolite composition, ultramafic cumulates, and ophicarbonate rocks (Bortolotti et al., 1994; Tartarotti & Vaggelli, 1994; Viti & Mellini, 1998). The Elba serpentinites consist of lizardite, chrysotile, magnetite, and carbonates produced by mid-ocean ridge serpentinization and are associated with chrysotile vein and antigorite shear veins (Viti & Mellini, 1996, 1997, 1998). The serpentinite complex preserves a wide range of structures, including mylonitic fabrics related to the Jurassic spreading phase (Frassi et al., 2017) and serpentine-rich fault rocks reworked by Apennine out-of-sequence thrusts (Papeschi et al., 2021; Viola et al., 2018). The oceanic sediments are Middle/Upper Jurassic-Lower Cretaceous radiolarian cherts (Diaspri Fm.), Lower Cretaceous limestone turbidites (Calpionelle limestones Fm.), and shales with limestone layers (Palombini shales Fm.). The Palombini shales (Figure 2), referred to the Hauterivian-Albian (~133–100 Ma; Principi et al., 2015) are the youngest formation of the Ophiolitic Unit. Pandeli et al. (2001) investigated the metamorphism of the Ophiolitic Unit through the analysis of the illite crystallinity on the Palombini shales, characterized by the illite + chlorite + vermiculite + quartz + feldspar ± chlorite ± calcite assemblage, obtaining $\Delta 2\theta$ values between 0.41 and 0.51, indicative of deep diagenetic to low anchizone conditions (T ~ 150–200°C).

3. Tectonics of the Ligurian Units on Elba

The Ophiolitic Unit consists of multiple basement-and-cover repetitions (or subunits) which share a common ENE-vergence. Perrin (1969, 1975) recognized at least four subunits stacked on W-dipping top-to-E thrusts and characterized by N-S to NNW-SSE striking upright to E-verging tight to isoclinal folds (Figures 2 and 3). Internally, these subunits largely preserve the stratigraphic relationships between sedimentary formations and the ophiolitic basement. Keller & Pialli (1990) and Keller and Coward (1996) ascribed these structures to the accretion of oceanic units in the Ligurian prism during the Cretaceous-Eocene. A sudden change in deformation style marks the base of the Ophiolitic Unit, where a series of Ligurian-derived tectonic slices lie at the contact between the overlying ocean-derived nappes and the underlying continent-derived units (Figures 2 and 3b). These slices occur under a top thrust, marked by intensely deformed serpentinites and comprise N-S striking and W-dipping lenses of sedimentary formations—predominantly Palombini shales—surrounded by deformed serpentinites (Figures 2 and 3b). Perrin (1975) defined this structure as tectonic slices and interpreted them as a zone of strong tectonic lamination in the reverse limbs of folds. Keller & Pialli (1990) interpreted them as duplexes, recognizing the presence of blocks and olistoliths of ophiolitic material in the Palombini shales at the base of the prism. Indeed, one of the notable features of Eastern Elba is the occurrence of the Palombini shales, the youngest formation affected by prism deformation, only at the base of the Ophiolitic Unit, mostly as tectonic slices or in the reverse limb of a large fold in the northernmost part of the island (Figures 2 and 4). In the following text, we refer to this complex of tectonic slices as the Norsi-Cavo Complex (NCC), named after the geographic names of its northernmost and southernmost outcrops (Figure 2). The more recent (late Miocene–early Pliocene) Zuccale Fault locally interrupts the NCC, displacing it 6 km to the east (Figure 3b). Nevertheless, the NCC can be traced from the footwall of the Zuccale Fault in Norsi to the southwest to its hanging wall, from Porto Azzurro to the south to Cavo in the north (Figures 2 and 3b). Along this interval, which exposes 10–12 km of along-strike variations of the NCC, the NCC varies in thickness from some tens of meters to about half a km (30–600 m; Figure 3b). Overall, the style of deformation varies from a tectonic mélange in Cavo to a complex of tectonic slices separated by shear zones in the rest of the NCC, well exposed in the area of Norsi. In the following text, we, therefore, focus on the description of the NCC in the excellent coastal outcrops of (a) Cavo, and (b) Norsi (Figure 2).

3.1. The Cavo Section

The ~1 km long coastal section between Capo Vita and Capo Castello exposes the contact between oceanic rocks to the west (Palombini shales, part of the Ophiolitic Unit), and the underlying Tuscan Nappe, to the east (Figure 4a). Here, the Tuscan Nappe consists of Upper Cretaceous-Eocene limestones and varicolored slates (Scaglia Toscana

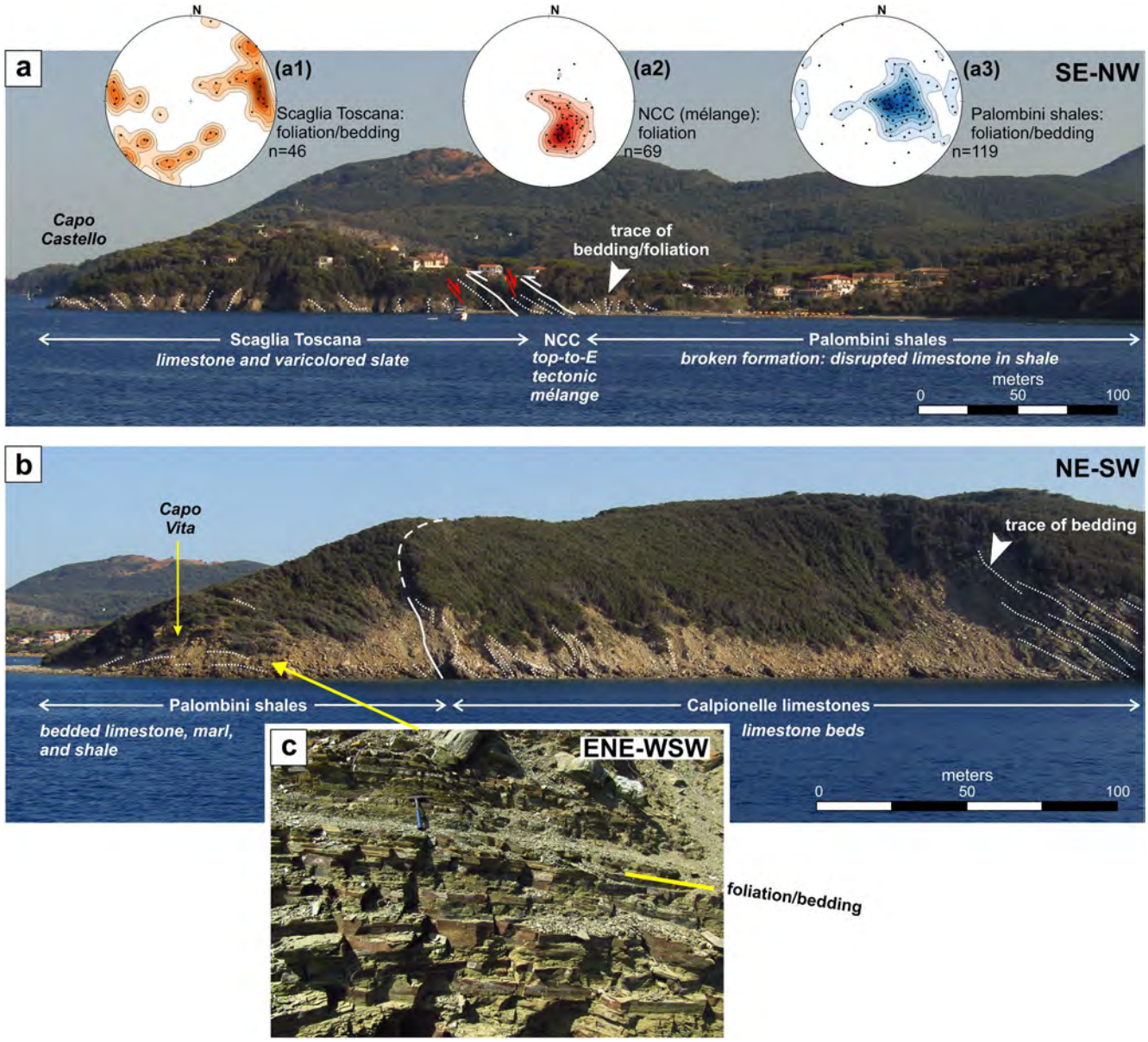

Figure 4. The cross section of Cavo. (a) Panoramic view of the contact between the footwall block (Scaglia Toscana) and the hanging wall block (Palombini shales) of the top-to-E shear zone marked by the Norsi-Cavo Complex (NCC). The stereonets here (a1, a2, and a3) and in the following figures are equal area, lower hemisphere projections that show contoured poles to planar elements and linear elements. (b) Stratigraphic contact between the Palombini shales and the Calpionelle limestones at Capo Vita and (c) detail of the rhythmic alternations of limestone, shale, and marls and parallelism between foliation and bedding in the Palombini shales therein.

Fm.) and Oligocene foredeep turbidites (Macigno sandstone) (Figure 4a; Perrin & Neumann, 1970; Keller & Pialli, 1990; Massa et al., 2017). The rocks of Cavo were also interpreted as a separate unit from the Tuscan Nappe (Grassera Unit; Principi et al., 2015). However, there is no difference in metamorphic grade between the rocks of Cavo and the rest of the Tuscan Nappe, as shown by the illite crystallinity data of Pandeli et al. (2001). The contact between oceanic and continental units occurs through a 30–40 m thick serpentinite mélange zone, previously interpreted as a rotated top-to-E extensional shear zone (Bianco, 2020; see discussion), which we re-assign to the Norsi-Cavo Complex (NCC; Figure 4a). Along the section, foliations, bedding planes, and tectonic contacts dominantly strike N–S to NE–SW, dipping gently to moderately to the WNW–NNW (stereonets a1, a2, a3 in Figure 4a). The Tuscan Nappe shows WSW-dipping foliations (stereonet a1 in Figure 4a) with a scattering related to the presence of type 3 interference folds *sensu* Ramsay & Huber (1987) (Elter & Pandeli, 2001). The Palombini shales lie in the inverted limb of a km-scale fold, underneath the W-dipping contact with the older

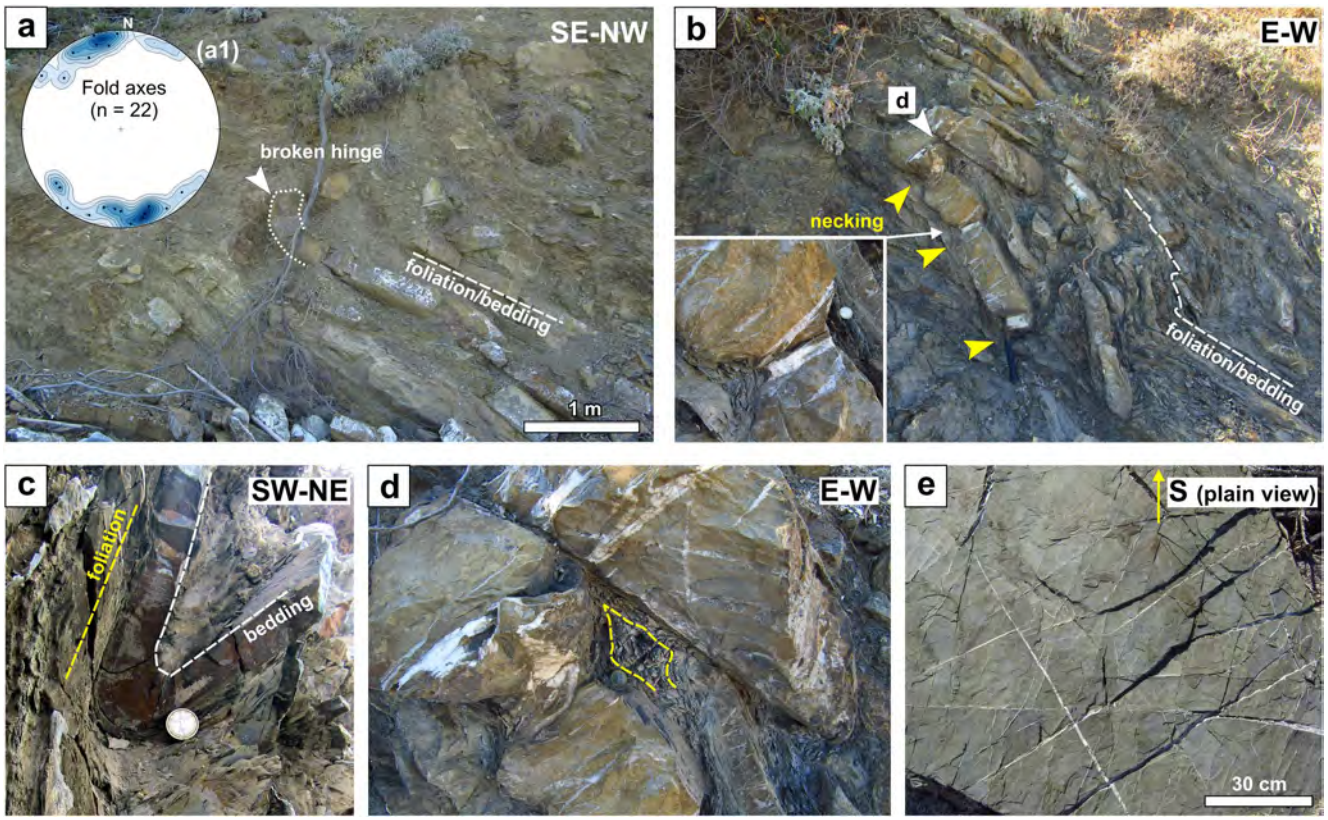

Figure 5. Deformation features in the Palombini shales broken formation in Cavo. (a–b) Disrupted limestone layer and broken fold hinges in outcrops with (a) low limestone to shale ratio and (b) high limestone to shale ratio. The inset highlights a detail of boudinaged limestone with blocky calcite veins in the necks in (b). a1: inset stereonet showing the trend/plunge of fold axes in the Palombini shales. (c) Tight fold developed in a limestone layer surrounded by shale. Note the parallelism between the foliation and the axial plane of the fold. (d) Detail of (b) showing complex folding of the shale between the limestone blocks (yellow dashed line = foliation). (e) Plain view of a limestone layer, variably crosscut by white, blocky carbonate veins.

Calpionelle limestones exposed to the NW, in Capo Vita (Figure 4b). Illite crystallinity data reveals the presence of a metamorphic step in the Cavo section, with the Palombini shales yielding $\Delta 2\theta = 0.41–0.51$ (high diagenesis/anchizone), whereas the Scaglia Toscana Fm. marked by $\Delta 2\theta = 0.25–0.39$ (anchizone; Pandeli et al., 2001).

3.1.1. The NCC Hanging Wall: Deformation of the Palombini Shales in Cavo

The Palombini shales show variability in their structural style along the 1 km NW–SE oriented section from the stratigraphic contact with the Calpionelle limestones (Figure 4b) to the tectonic contact with the underlying NCC (Figure 4a). Close to the Calpionelle limestones, the Palombini shales preserve their lateral continuous beds of alternating limestones, marls, and shales organized in a gently to moderately WSW-dipping monocline (Figure 4c). The shales and the marls are characterized by a WSW-dipping scaly fabric/slaty cleavage generally oriented parallel to bedding. Sets of blocky carbonate veins with variable orientation crosscut the limestone layers. Bedding-parallel veins are also present at the contact between the limestones and shales/marls layers.

The lateral continuity of bedding is lost in the lower part of the section, approaching the tectonic contact with the NCC (Figure 4a). There, and for ~500 m in thickness, most of the Palombini shales crop as a broken formation with blocks and lenses of disrupted limestone layers surrounded by shales with a scaly fabric (Figures 5a and 5b). The deformation style appears to depend on the limestone to shale ratio. Where shales dominate, blocks and lenses of limestone with a lateral continuity of a few meters occur isolated within a shaly matrix (Figure 5a). On the other hand, where limestone is more abundant, the disrupted limestone layers are arranged into complex folds, boudins, and inverted boudins (i.e., folded boudins), as the limestone blocks interacted during deformation (Figure 5b). This structural variability also influences the geometry of folds, which range from non-cylindrical folds affecting both limestone and shale in limestone-rich outcrops (Figure 5b) to isolated, rootless folds' hinges developed in limestone where the shale matrix dominates (Figure 5a). In both situations, folds show constant

N–S to NNW–SSE trending axes with moderate 0–15° plunge toward the N and the S (stereonet a1 in Figure 5a) and tight to isoclinal geometry with recumbent to W-dipping axial planes (Figure 5c). Boudinage structures are common where the limestone to shale ratio is high (Figure 5b). Boudins show variable geometry, ranging from symmetric pinch-and-swell structures to asymmetric boudins (Figure 5d), with blocky carbonate veins concentrated in the necks (Figure 5b). In many cases, the boudins appear folded and slightly rotated (e.g., Figure 5b). Passive, complex disharmonic folding of the scaly fabric characterizes the shale interlayers that occur between the boudinaged limestone blocks and the localized shear structures that accommodated the relative movement of the blocks (Figure 5d). A network of blocky carbonate veins, with thickness ranging from 1 to 2 mm to about 5–6 cm, affects the limestone layers (Figure 5e), independently from boudinage structures (Figure 5b). Carbonate veins appear considerably rarer in outcrops dominated by shales (e.g., Figure 5a).

3.1.2. The Cavo Mélange Zone

In Cavo, the 30–40 m-thick serpentinite-derived mélange belonging to the NCC corresponds to a shear zone (Figures 6a and 6b) that separates the Palombini shale (hanging wall block) from the Scaglia Toscana Fm. (footwall block; Figure 4a). In the field, the contact of the serpentinite mélange with the overlying Palombini shales appears as a cemented hardground, consisting of strongly veined, ophicarbonate with fragments (range: <1–20 cm) of limestone, shale, and marl (Figure 6a). At the base, the contact is marked by an abrupt transition between the mélange rocks and the underlying foliated metasandstone, slate, and metalimestone (Scaglia Toscana and Macigno Sandstone Fms.; Keller & Pialli, 1990) (Figure 6b). The mélange shows a block-in-matrix fabric with heterometric blocks and fragments of ultramafic, mafic, and sedimentary rocks surrounded by a carbonate-rich serpentinite-derived matrix (Figures 6c and 6d). The foliation of the mélange matrix is defined by subparallel serpentine-rich bands of various color (greenish to dark green/black), carbonate veins, trails of angular blocks, and whitish talc-rich bands (Figure 6d). Lineations are rare and highlighted by quartz or carbonate rods and aggregates of phyllosilicates or opaque minerals, oriented NW-SE (inset in Figure 6d). The foliation varies in spacing and intensity across the mélange, with strongly foliated bands (Figure 6c) that alternate with domains where the foliation is folded, irregular, and more spaced, as it bends around the blocks (Figure 6d). Despite these irregularities, the foliation dominantly strikes NW–SE to E–W, dipping to the NNW (stereonet a2 in Figure 4a). Boudinaged carbonate veins with millimetric thickness occur oriented parallel to the foliation, but we observe also younger carbonate veins cutting through the mélange.

The blocks show variable size, shape, and composition. Fractured serpentinites form the largest blocks that we observed ranging in size from 0.5 to 3–4 m (e.g., Figure 6c), but the vast majority are between a few mm and 20 cm (Figure 6d). The most abundant blocks are ultramafic (serpentinite and ophicarbonate rocks) and sedimentary (limestone and subordinate marl and shale), while blocks of mafic rocks are the least common (Figures 6e–6h). Irregular networks of mm- to cm-thick carbonate and serpentine veins (e.g., Figure 6d) and discrete shear fractures break the larger (>0.5 m) ultramafic blocks. The smaller ultramafic fragments typically show an angular outline (e.g., Figure 6f). Limestone, shale, and mafic blocks tend to display a rounded shape, delimited by reaction rims and/or carbonate veins (Figure 6e): mafic blocks usually show light green rims, while limestone blocks have dark green to black rims (Figures 6g and 6h). Carbonate veins, with mm- to cm-thickness, are common around these rims, mantling the blocks and appearing thicker in the direction parallel to the foliation, similar to mesoscopic pressure shadows (Figure 6e). Limestone blocks often contain networks of blocky carbonate veins crosscut by reaction rims, suggesting that these veins formed before the reaction rims and possibly before the Cavo mélange (Figure 6g). The structural style of the veined limestone blocks and the observed composition of the sedimentary fragments (limestone, marl, and shale) allows us to consider the sedimentary blocks as derived from the overlying Palombini shales (Figure 5).

Several kinematic indicators within the mélange indicate a dominant top-to-SE sense of shear. Many limestone blocks mantled by reaction rims shows an asymmetric shape that indicates an eastward sense of shear (Figure 6h). Asymmetric boudinage structure occurs in some blocks that are displaced by several cm to the east along subhorizontal shear bands (Figure 6i). Shear band structures (S-C fabrics) are also very common in the mélange matrix, where the NNW–NW dipping foliation is cut and dragged eastwardly by subhorizontal C' shears (stereonet i1 in Figure 6i). The angle between the S foliation and C′ shears is generally around ∼30°. Since lineations are mostly absent/not evident in the mélange, the strike of the plane perpendicular to the bisector of S and C′ structures is the most reliable indicator of the direction of shearing, oriented NW–SE (stereonet i1 in Figure 6i). Additional kinematic indicators are represented by asymmetric aggregates of talc and carbonates occurring in the mélange

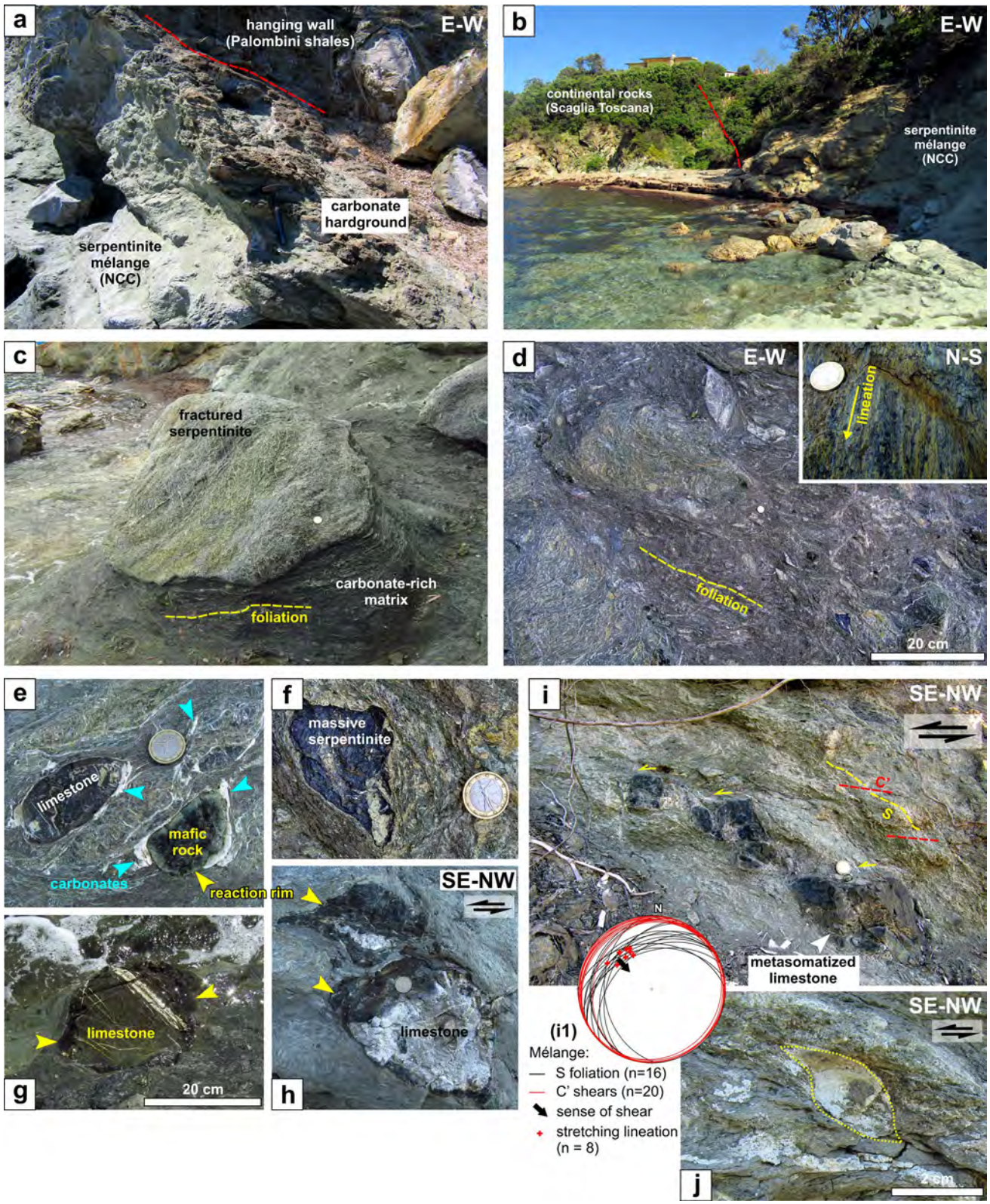
a
hanging wall
(Palombini shales)
E-W
carbonate
hardground
serpentinite
mélange
(NCC)
b
E-W
continental rocks
(Scaglia Toscana)
serpentinite
mélange
(NCC)
c
fractured
serpentinite
carbonate-rich
matrix
foliation
d
E-W
N-S
lineation
foliation
20 cm
e
limestone
mafic
rock
carbonates
reaction rim
f
massive
serpentinite
SE-NW
limestone
g
limestone
20 cm
h
i
SE-NW
C'
S
N
metasomatized
limestone
(i1)
Mélange:
S foliation (n=16)
C' shears (n=20)
sense of shear
stretching lineation
(n = 8)
SE-NW
2 cm
j

Figure 6.

matrix, with σ-like shape, consistent with top-to-SE sense of shear (Figure 6j). Independently, the study by Bianco (2020) confirms the top-to-SE kinematics of the mélange documenting also the presence of late top-to-W faults overprinting the top-to-SE structures.

3.2. The Norsi Section

The Norsi area offers a 1.5 km long coastal exposure across the NCC at the base of the Ligurian Units. The NCC here consists of a series of tectonic slices of NW-dipping Palombini shales coupled with tectonized ultramafic rocks (serpentinites, serpentinized peridotites, and ophicarbonate rocks; Figures 2 and 7). Their total thickness varies between 100 and 500 m, while the shale slices range between a few meters to ∼100 m. The contact between the Palombini shales and the serpentinites (Figure 7) is marked by a network of anastomosing shear zones, that range in thickness from less than a meter to several tens of meters. These shear zones overprint older deformation features developed in both the Palombini shales and the serpentinites (described in the next paragraphs). These shear zones, including foliations and tectonic contacts, dip generally to the NW, concordantly with the overlying Ophiolitic Unit (Figure 7). The upper contact of the NCC fades within the serpentinites of the Ophiolitic Unit, which in turn preserve primary contacts with gabbro and basalt sequences covered by sedimentary sequences (Figure 7). At the cartographic scale, the Ophiolitic Unit and the NCC are involved in a series of open recumbent folds with hundreds of meters wavelength and NNE–SSW trending axes (cross section in Figure 7).

The base of the NCC is locally crosscut by a NW-dipping top-to-E out-of-sequence thrust (the CN-MAT in Figures 2 and 7; Viola et al., 2018) which in Norsi brings the NCC, originally outside of the contact aureole of the Porto Azzurro pluton, in contact with cordierite-bearing aureole rocks of the Ortano Unit. Consequently, the base of the NCC does not preserve its original relationships with the underlying continent-derived units in Norsi. The NCC escaped contact metamorphism, but was locally affected by channelized, hydrothermal fluids with the development of calcsilicates in reactive limestone layers within the Palombini shales and in some serpentinite bodies (Zucchi, 2020).

3.2.1. Deformation of the Palombini Shales at Norsi

The Palombini shales show a heterogeneous distribution of deformation and an internal variation in structural style (Figure 8). The shales and marls are characterized by a slaty cleavage, that is generally parallel or sub-parallel to the limestone layers. Limestones generally lacks cleavage planes, although locally they show pressure solution surfaces and/or stylolites oriented parallel to foliation. Bedding-parallel blocky and fibrous carbonate veins, showing extensional to hybrid mode of opening, are common. Fibers in carbonate veins are oriented perpendicular to the vein walls, hence generally perpendicular to the foliation, and do not mark a specific stretching direction. Furthermore, irregular networks of chocolate-tablet-like blocky carbonate veins commonly crosscut limestone layers. The foliation generally strikes N–S to NE–SW and dip moderately (10–50°) to the NNW–NW (stereonet a1, a3, and a5 in Figure 7), with local southeastward dips caused by the presence of late open folds with inclined to recumbent geometry shown in the cross section of Figure 7. Such open folds correspond in structural style to those refolding the entire nappe stack (visible in Figure 3b) and are, hence related to the post-nappe stacking (Miocene) deformation stage. The scattering of the poles to the foliation (stereonet a1 and a5 in Figure 7) is consistent with roughly NW–SE trending axes of such late folds. Locally, shaly layers show subhorizontal crenulations (stereonet a6 in Figure 7) that can be geometrically linked to the axial plane foliation of these folds.

The structural style of the limestone-shale multilayer appears related to the thickness of the limestone beds and the proportion of limestone over the surrounding shales. Bedding is well preserved in outcrops where thick limestone layers (0.5–2 m) alternate with thin shale interlayers (Figure 8a). These outcrops are typically affected by high wavelength open to tight folds and local, incipient boudinage of the limestone layers. Outcrops with thin

Figure 6. The mélange of the Norsi-Cavo Complex (NCC) in Cavo. (a) Detail of the upper contact between the mélange and the Palombini shales, marked by a carbonate-rich zone (hardground). (b) Detail of the main body of the mélange and its basal contact with the Scaglia Toscana Fm. (Cavo Fm.) (c) Large block of fractured and veined carbonate-rich serpentinite surrounded by the mélange matrix. (d) Detail of the mélange matrix, consisting of carbonates and serpentine and showing a foliated fabric enveloping heterometric blocks of ultramafic, sedimentary, and mafic rocks. Carbonate veins are mostly folded or parallel to the foliation, but some crosscut the mélange fabric. The inset highlights a foliation surface showing well-developed mineralogical lineations (phyllosilicate and opaque trails). (e–h) Examples of blocks/fragments encased in the mélange, showing (e, g, h) reaction rims (yellow arrows), (e) marginal carbonate veins (cyan arrows), and (g) internal carbonate veins crosscut by the mélange matrix. (h, i, j) Top-to-E kinematic indicators: (h) asymmetric blocks, (i) blocks crosscut by C′ shears and S-C′ structures, and (j) asymmetric aggregates of talc (yellow dotted line). i1: S-C′ foliation planes.

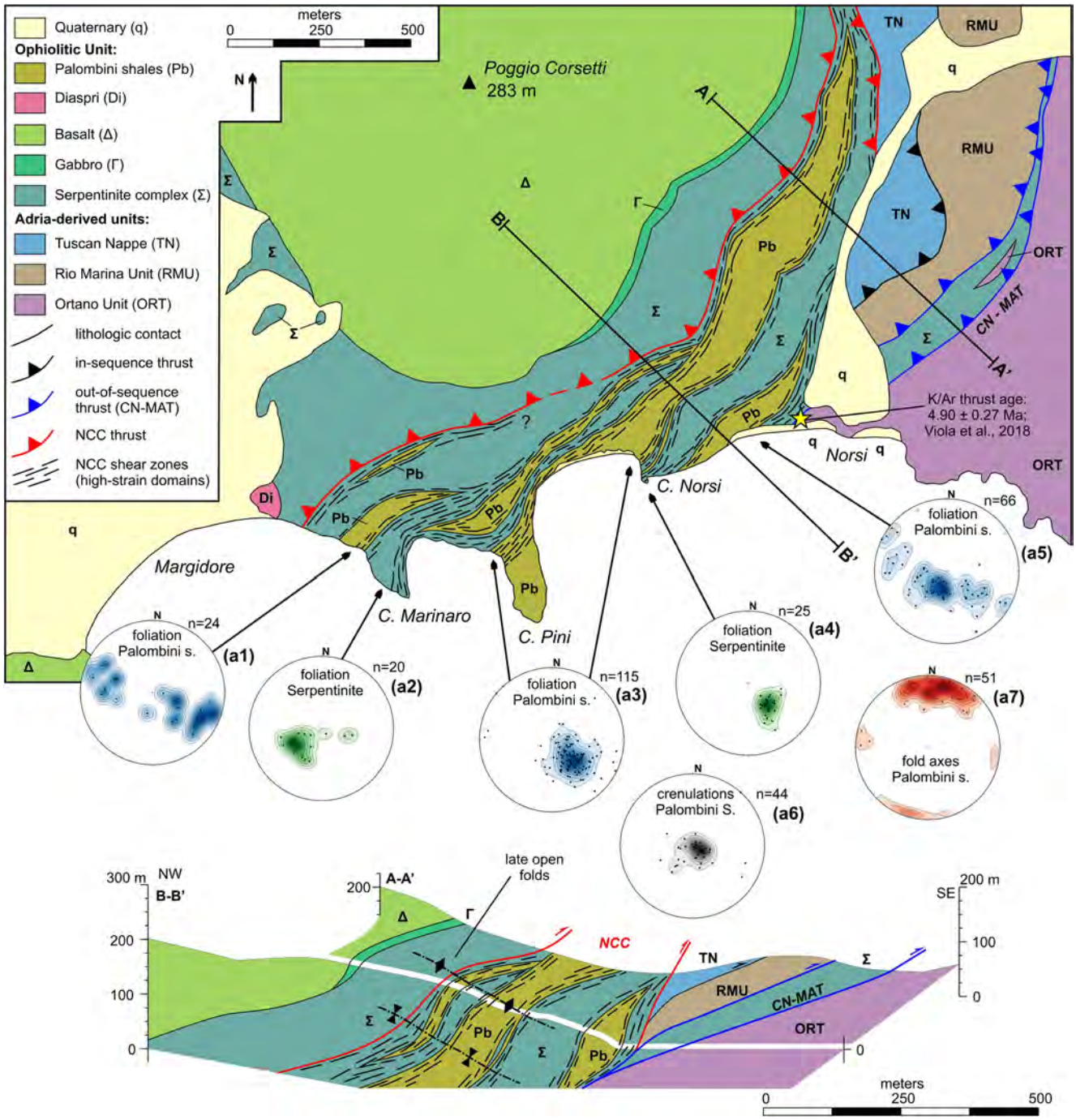

Figure 7. Geologic sketch map and composite cross sections of the Norsi area with (a1–a7) stereonets to the main structural features. Map after Barberi et al. (1967), improved based on field surveying carried out in the present work. The location of the fault gouge sample dated via K/Ar by Viola et al. (2018) is shown with a yellow star.

limestone layers (<10 cm) and roughly equal proportion (i.e., rhythmic alternations) of shale and limestone show disharmonic folds with thickened hinges and local boudinage of the limbs (Figure 8b). The hinges of these folds commonly show extensional veins fanning through their outer arc. Moreover, these outcrops notably display refolded folds and overprinting axial plane cleavages (Figure 8b), which are likely the result of progressive deformation during the same deformation phase. Indeed, we note that the orientation of the axes, axial planes, and geometry of these folds is identical (see below). Where, the Palombini shales are shale-dominated, the most

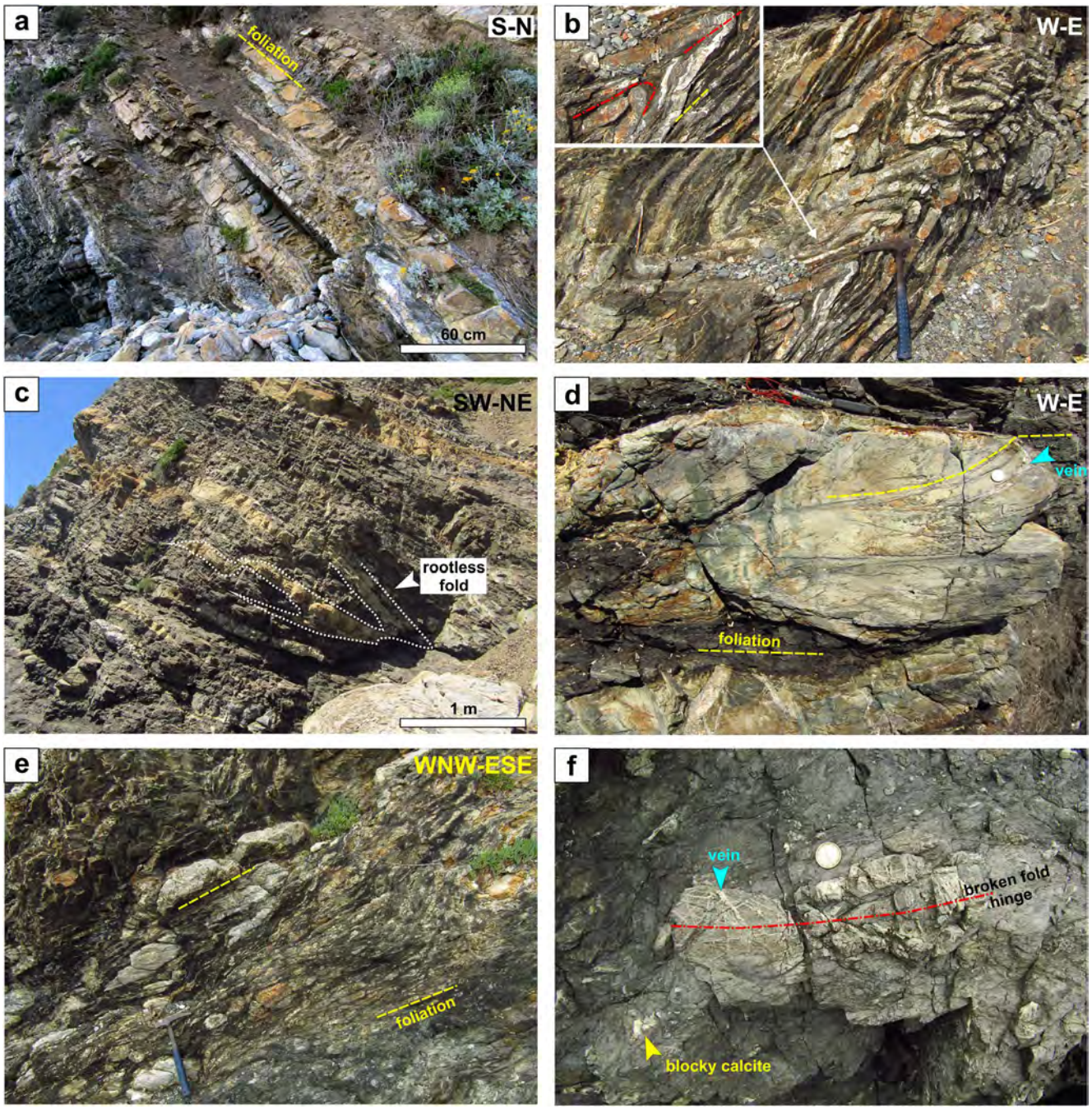

Figure 8. The Palombini shales in Norsi. (a) N-dipping, thick limestone beds separated by thin shale layers. (b) Rhythmic alternations of tightly interbedded limestone and shale with refolded folds (red dashed lines = traces of axial planes; yellow dashed line = foliation). (c) Rootless folds in partially disrupted limestone beds in a shale-dominated outcrop. (d) Thickened hinge in limestone with refracted axial plane foliation and a carbonate vein cutting through (cyan arrow). (e) Contact between intact and disrupted Palombini shales with (f) detail of folded limestone clast crosscut by networks of veins, surrounded by a shaly matrix.

common situation, disrupted lenses of limestone of variable thickness are laterally continuous only for some meters up to some tens of meters (Figure 8c). In shale-dominated outcrops folds develop in limestone layers: they are rootless (Figure 8c) and show overthickened hinges and tight to isoclinal interlimb angle (Figure 8d). Cleavage refraction may be visible in clay-bearing limestone layers, and foliation-parallel veins may cut through the hinge (Figure 8d). Despite the internal variability, these folds show remarkably similar orientation of fold axes: they dominantly trend NNW–SSE and plunge gently to moderately (0–25°) to the NNW (stereonet a7 in

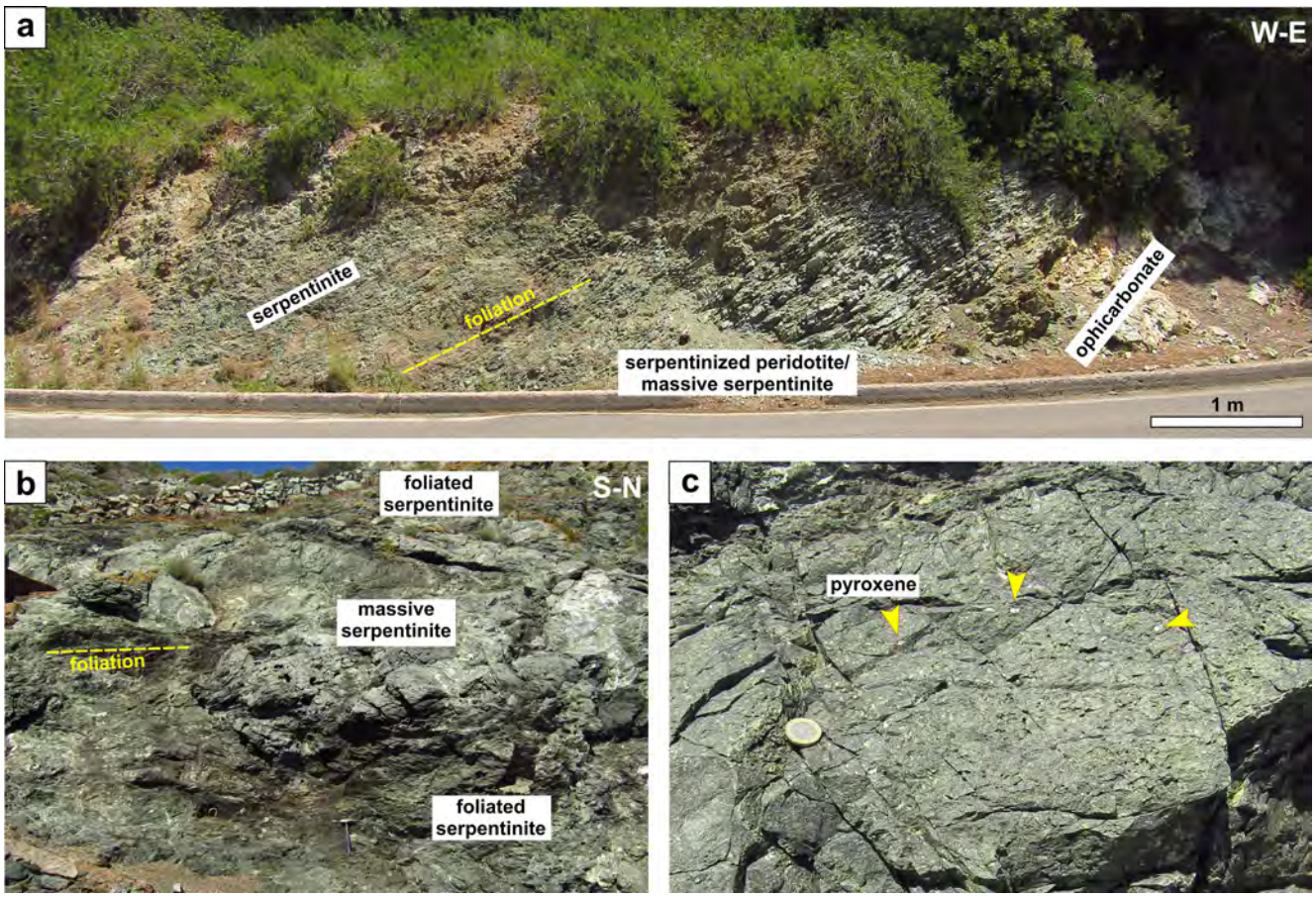

Figure 9. Fabrics of the Norsi serpentinites. (a) Road cut showing the compositional variability within the ultramafics. (b) Outcrop of foliated serpentinite with lenses of massive serpentinites. (c) Detail of strongly serpentinized peridotite preserving some pyroxene relics (likely bastites).

Figure 7), with axial planes inclined to the WNW (e.g., Figure 8b), recumbent or NE-dipping (Figures 8c and 8d). At the contact with the serpentinites, the margins of the Palombini shales lenses are often characterized by metric to tens of meters-thick zones of chaotic fabric resulting from intense deformation (Figure 7). The block-in-matrix structures occur at the expense of the Palombini shales irrespectively of their limestone to shale ratio and bed thickness. The example shown in Figure 8e documents the quite abrupt contact between intact rhythmic alternation of limestone and shale (left) with a thickness of ~5–20 cm and disrupted, chaotic fabrics (right). The orientation of the foliation is constant across the transition between the two fabrics (Figure 8e). Chaotic fabrics contain heterogeneously sized blocks (mm- to dm) entrained in a shale matrix (Figures 8e and 8f). The blocks consist of angular fragments of limestone that internally preserves several tectonic structures like networks of blocky carbonate veins, and broken fold hinges (Figure 8f). Notably, fragments of blocky calcite, likely derived from disrupted veins, occur in the mélange matrix (Figure 8f).

3.2.2. Structural Fabrics of the Serpentinites at Norsi

The serpentinites at Norsi show a wide range of different fabrics, all oriented parallel to the dominantly W to NW-dipping regional foliation (Figure 7) as in the rest of the island (e.g., Papeschi et al., 2021), Specifically, in the Norsi area the attitude of the serpentinites varies from NW- to NE-dipping, due to the presence of late open recumbent folds affecting the sequence (stereonet a2 and a4 in Figure 7). As shown in Figure 9a, the ultramafic rocks (*sensu latu*) consist of parallel bodies/lenses of serpentinite, serpentinized peridotite (preserving a few pyroxene and spinel relics), and ophicarbonate rocks. The foliation in the ultramafic rocks is defined by the preferred orientation of serpentine, olivine and pyroxene relics, and serpentine veins (e.g., Figure 9a). The serpentinite foliation is often irregular or curvilinear, enveloping around lenses and bodies of unfoliated or poorly foliated ultramafic rocks (serpentinite and strongly serpentinized peridotite), resulting in lens-like structures,

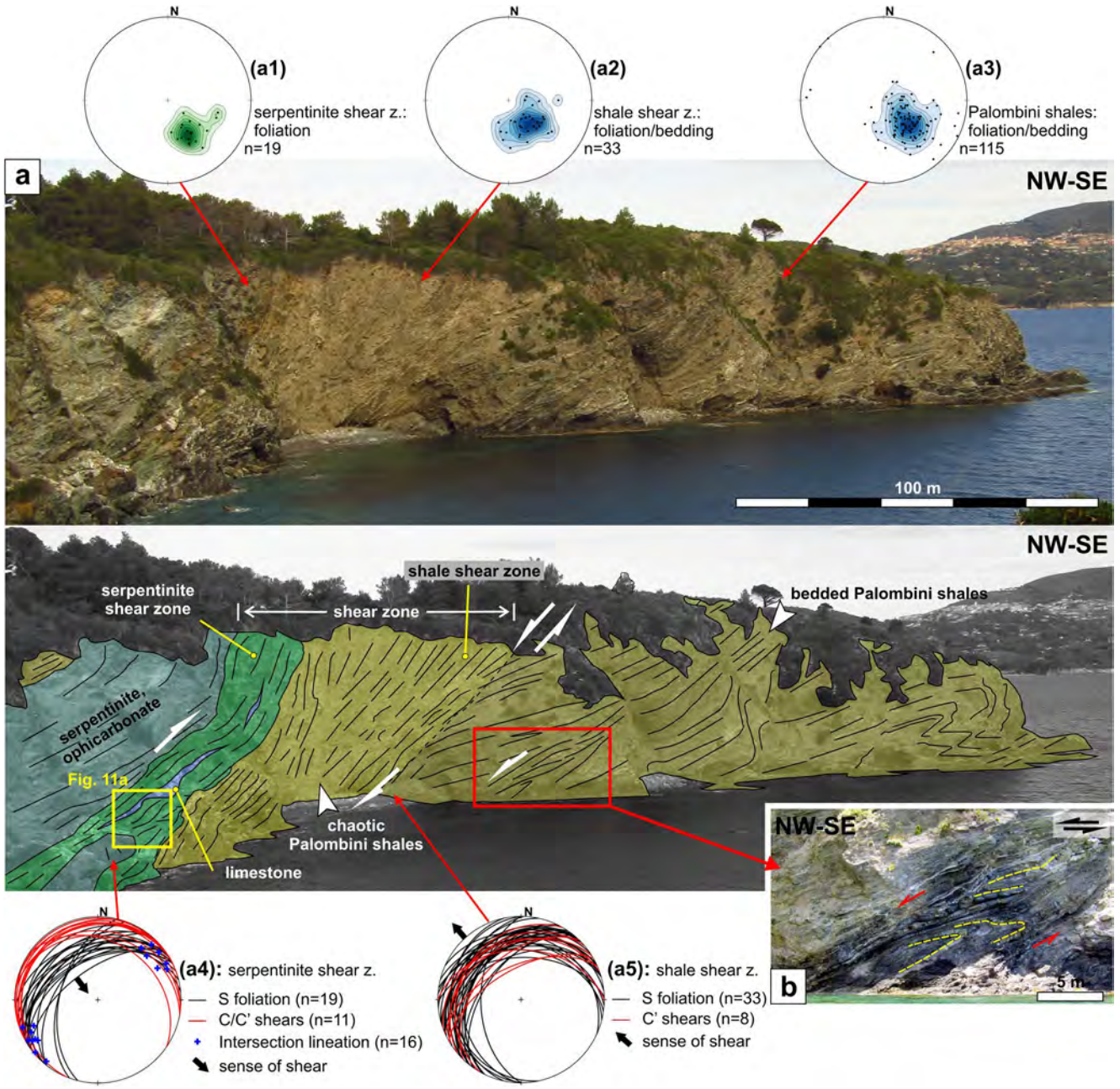

Figure 10. The top-to-SE shear zone at Capo Pini. (a) Panoramic view of the shear zone with (a1–a5) stereographic projections showing the orientation of the main structural elements. (b) Detail showing NE-verging folds and layers, boudinaged and drag along W-verging shear zones.

commonly observable at outcrop scale. Serpentinized peridotites/massive serpentinites can show a spaced foliation, outlined by foliated serpentine-rich bands as in Figure 9a, but—more commonly in the Norsi area—they occur as unfoliated bodies (Figure 9b) crosscut by serpentine veins and containing a few relics of mm- to cm-sized pyroxene grains (Figure 9c).

3.2.3. Deformation in the NCC Shear Zones in Norsi

The anastomosing shear zones of the NCC that separate the slices of Palombini shales from the serpentinites are well-exposed in several coastal sections in the Norsi area (Figure 7). In Figures 10 and 11, we show in detail a complete section though one of these shear zones in the C. Pini—C. Marinaro area, coupling ultramafic rocks (hanging wall block) with the Palombini shales (footwall block). This shear zone is ~40–50 m thick and

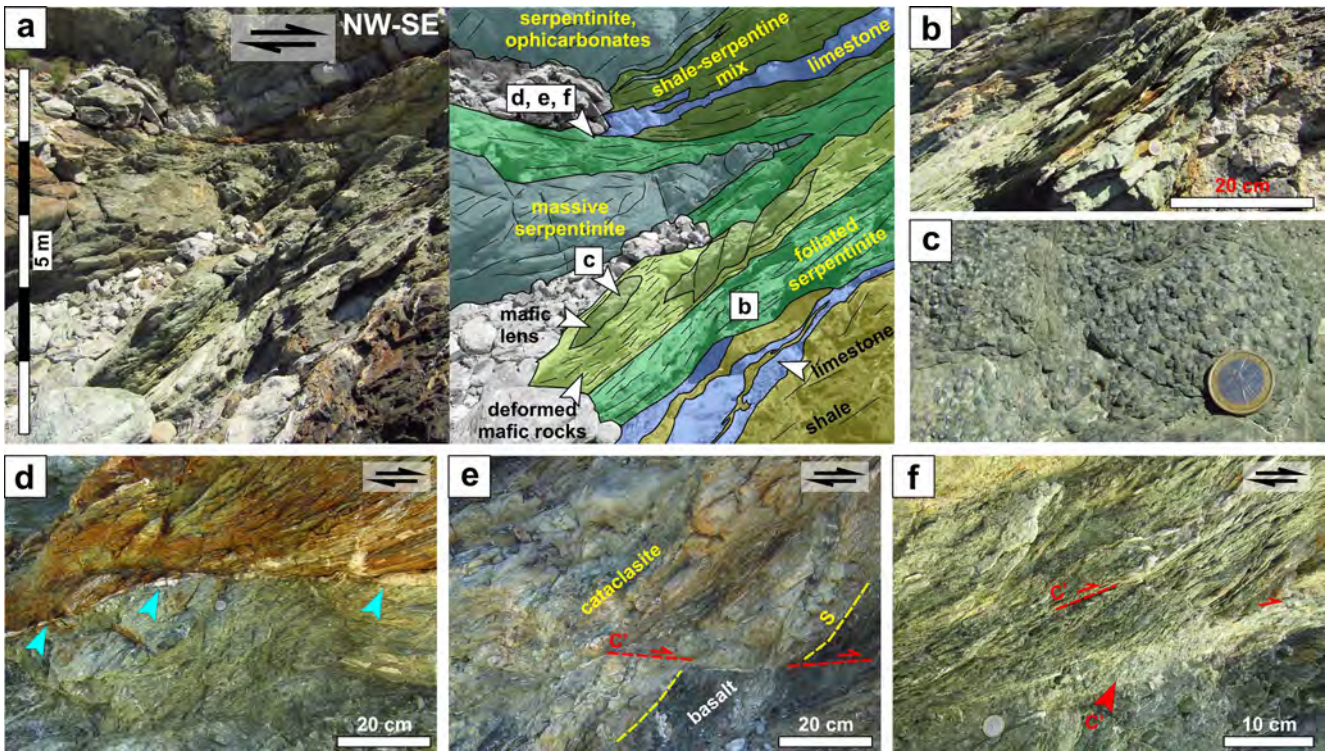

Figure 11. The upper part of the Capo Pini shear zone (serpentinite shear zone in Figure 10). (a) Close up of the shear zone and detail of the lithologies involved. (b) Contact between the Palombini shales (below) and the serpentinites (above). Note the strongly foliated fabric of the serpentinite. (c) Spherulites in the core of the mafic block. (d–f) Top-to-E kinematic indicators with (d) deflected carbonate vein (cyan arrows), (e) S-C′ structures affecting mafic blocks, and (f) cataclastic bands oriented parallel to C' shears.

comprises an upper 5–10 m thick serpentinite-rich part, developed in contact with the hanging wall lithologies (serpentinite and ophicarbonates), in sharp contact with a lower 20–30 m thick shale-rich part developed in the Palombini shales (Figure 10a). Foliations, from the footwall to the hanging wall blocks concordantly dip to the NNW–NW (stereonet a1, a2, a3 in Figure 10a). The basal contact of the shale-rich part of the shear zone (shale shear zone) truncates the Palombini shales, characterized by a NW-dipping slaty cleavage and shale/limestone layering, locally refolded by ESE-verging tight to isoclinal inclined folds (visible to the right in Figure 10a). As shown in Figure 10a, the contact with the overlying shale shear zone is marked by a top-to-NW drag of the foliation in the Palombini shales and extensive boudinage of lenses of limestone and shales, whose asymmetric shape is consistent with top-to-NW sense of shear (Figure 10b). The shale shear zone is characterized by a chaotic block-in-matrix fabric with disrupted blocks of limestone surrounded by a shaly matrix with a penetrative scaly fabric (Figure 10a). S-C′ structures and drag folds in the shaly shear zone indicate top-to-NW kinematics with C' shear bands being statistically steeper to the NW than the shear zone foliation (stereonet a5 in Figure 10).

The overlying serpentinite-rich part of the shear zone (serpentinite shear zone) consists of a complex mixture of deformed ultramafic, mafic and sedimentary rocks encased in foliated serpentinites (Figure 10a). We investigated in detail the outcrop of Figure 11a, which offers a full section from the top of the sheared Palombini shales (shale shear zone) to the base of the hanging wall block. The foliation of the disrupted Palombini shales at the base is generally sub-parallel to the shear zone foliation but limestone layers are locally truncated by the overlying serpentinites (Figure 11a; detail in Figure 11b). Most of the shear zone consists of strongly foliated serpentinites (Figure 11b) with S-C′ structures. Their foliation is defined by the preferred orientation of serpentine and carbonate veins occurring in the serpentinites (Figure 11b). The serpentinites in this section envelope a deformed mafic rock lens and a fractured, massive serpentinite body (Figure 11a). The mafic rock lens is truncated by NW-dipping high-angle domino type boudinage structures that indicate top-to-E sense of shear (Figure 11a). The mafic rock contains spherulitic textures (Figure 11c) in its core, which is mantled by foliated mafic material (Figure 11a). The massive serpentinite body variably preserves serpentinized minerals (pyroxene/olivine relics) and it is crosscut by serpentine and carbonate veins. The upper part of the shear zone consists of

a foliated greenish clay—serpentine mixture (mixed layer) that contains lenses of limestone (Figure 11a). The contact between serpentine-dominated and serpentine-clay lithologies is shown in Figure 11d. The mixed layer is in sharp contact with the overlying ultramafics, consisting of serpentinites and unfoliated ultramafic breccias rich in carbonate veins (ophicarbonates in Figure 11a). Figures 11d–11f show the complexity of the shear zone, which include well-foliated serpentinites, mafic rocks, and layers of serpentine- and carbonate-rich breccias and variably consolidated gouge/cataclasites (e.g., Figure 11f). S-C′ fabrics localized on C/C′ shear bands and with cm to dm displacement are observable at all scales (Figure 11e). C/C' shears are sub-horizontal to gently NW-dipping, compared to the moderately NW-dipping shear zone foliation that marks the S-fabric (stereonet a4 in Figure 10a): the intersection lineation between S and C/C′ planes is well visible on the polished serpentinite foliation planes. These structures are consistent with dominant top-to-SE sense of shear. Blocky and fibrous carbonate veins with variable thickness (mm–cm) occur generally sub-parallel to the foliation (Figure 11d), and they are commonly dragged eastwardly by C/C′ shears.

4. Discussion

4.1. Genesis and Significance of the Norsi-Cavo Complex: A Fossil, Alpine Subduction Channel?

Our field-based structural analysis allows to define for the first time the existence of a zone of intense deformation, characterized by severe tectonic slicing, mélanges, and broken formations that marks the contact between the oceanic Ligurian prism and the continent-derived nappes in the Northern Apennines orogenic wedge on the Island of Elba (Figure 2). Previously, several authors also recognized the intense tectonization at the base of the Ligurian Units, suggesting this deformation to be related to the Cretaceous-Eocene subduction stage (Keller & Pialli, 1990; Perrin, 1975). The nappe stack of Elba also recorded several events of extension, compression, and out-of-sequence thrusting in the Miocene which modified the original architecture and that are currently object of debate (see recent reviews in Ryan et al., 2021 and Jolivet et al., 2021). However, these events neither can be responsible for the formation of the NCC neither substantially modified the architecture of the NCC, because:

1. The NCC consists solely of oceanic-derived material (serpentinites, ophicarbonates, limestone, shale, mafic rocks; Figures 2, 3, 6, 7, 10 and 11). Even where the NCC is juxtaposed to continental units (e.g., the Tuscan Nappe in Cavo and the Ortano Unit in Norsi; Figures 6 and 7), no material derived from the continental block can be observed within the shear zone. This is an indication that the main structuration of the NCC occurred when only ocean-derived material was available, pointing to its development during the oceanic subduction, before the arrival of the Adria continental margin (hence before the Oligocene–early Miocene, based on the age of the early Apennine foredeep deposits; Conti et al., 2020 and references therein). On Elba the youngest sediments below the Ligurian Units are the Macigno Sandstone (Oligocene) in the Tuscan Nappe, and the Spotted Schists of the blueschist-facies Ortano Unit, which recently yielded 31.6 ± 0.5 Ma (Oligocene) detrital zircon ages (Jacobs et al., 2018).
2. The youngest sediment incorporated in the NCC are the Palombini shales (Figures 6, 7, 10 and 11), which in this area are Hauterivian-Albian (Lower Cretaceous) in age (Principi et al., 2015). This indicates that the deformation observed in the NCC postdates the Lower Cretaceous. In the Northern Apennines the late Cretaceous-Eocene interval corresponds to the timing of oceanic subduction (Molli et al., 2008; Vignaroli et al., 2008; Marroni et al., 2010, 2017).
3. Younger structures, like the Zuccale Fault or the Capo Norsi-Monte Arco Thrust invariably crosscut the NCC, affecting oceanic and continental units alike, as well as the Miocene magmatic rocks and their contact aureole (Figures 2, 3 and 7; Collettini & Holdsworth, 2004; Jolivet et al., 2021; Keller & Coward, 1996; Keller & Pialli, 1990; Smith et al., 2011; Musumeci & Vaselli, 2012; Musumeci et al., 2015; Papeschi et al., 2021). Ar/Ar and K/Ar radiometric dating confirm the geological relationships observable at the outcrop scale, constraining their activity to the late Miocene–early Pliocene (Viola et al., 2018 and references therein). Furthermore, as shown in Figure 3a, the NCC is involved, together with the nappes above and below it, in an antiform associated with the late Miocene activity of structures interpreted as out-of-sequence thrusts (Massa et al., 2017).
4. The underlying continent-derived units show a prograde metamorphic gradient, with deeper units marked by higher pressure orogenic metamorphism (Tuscan Nappe: anchizone; Rio Marina Unit: greenschists; Ortano Unit: lawsonite blueschists at $P > 1.5$ GPa; Papeschi et al., 2020 and references therein). This situation can be explained thanks to the presence of exhumation-related shear zones (shown in Figure 3a), which are parallel

to orogenic thrusts, dip to the west, and have top-to-W sense of shear (Ryan et al., 2021). These shear zones are observed in the continental wedge but are missing in the overlying Ligurian Units.

The previous interpretation of a segment of the NCC in the Cavo area as an earlier extensional shear zone that was rotated by the more recent activity of the ZF (Bianco, 2020) is not consistent with the evidence, reported by Musumeci et al. (2015), that foliations have identical attitude above and below the ZF and that, hence, no block rotation linked to its activity is possible. We hereby discuss observations arising from the present study that support the interpretation of the Norsi-Cavo Complex (NCC) as a fossil subduction channel in the inner part of the Northern Apennines.

The structural position of the NCC in the nappe architecture, below the Ligurian prism and right above the Adria-derived continental units, is a first-order observation. This position makes the NCC the internal analog to the Sestola-Vidiciatico Unit, interpreted as a fossil subduction channel in the external Northern Apennines (Remitti et al., 2007; Vannucchi et al., 2008). On Elba, the base of the Ligurian prism consist of an Ophiolitic Unit, considered to be a coherent ophiolite-bearing unit accreted in the Ligurian prism (Keller & Pialli, 1990; Perrin, 1975; Principi et al., 2015). Indeed, the Ophiolitic Unit, as shown in Figures 2 and 3b, is characterized by large-scale tight to isoclinal folds that affect a more-or-less preserved succession and that are only locally reworked by thrusts, largely localized in the reverse limbs of folds. The transition to the underlying NCC marks an abrupt change in deformation style, as also noted by Perrin (1975) and Keller & Pialli (1990). The NCC is indeed characterized by intense tectonic slicing that coupled and repeated lithotypes like Jurassic serpentinites and Cretaceous sediments that were originally distant in the stratigraphy of the Ophiolitic Unit (Figure 3b). Notably, the deformation of the NCC is also characterized by the development of mélange bodies (Cavo; Figure 6) and metric shear zones with mixed sedimentary and serpentinite-derived material (Norsi; Figures 10 and 11). A similar deformation style, with the formation of mélanges and complexes of tectonic slices derived from the upper plate and from the subducting slab, has also been reported in subduction complexes exposed for example, in the Shimanto Belt of Japan (Kimura et al., 2012; Kitamura et al., 2005) and in the Alps (Angiboust et al., 2014, 2015; Bachmann, Oncken, et al., 2009; Bachmann, Glodny, et al., 2009; Ioannidi et al., 2020). Both in Norsi and in Cavo, the deformation structures linked to these fabrics are invariably characterized by top-to-E kinematic indicators, and N–S striking, E-vergent folds, associated with N–S to NE–SW striking and WNW–NNW dipping foliations (Figures 4, 5, 7, 8 and 10). The trend and vergence of these structural elements, typical of Apennine structures on Elba, are observed both in the Ligurian Units and the underlying continental units, and they are linked to the oceanic to continental convergence stage D_1 (Keller & Coward, 1996; Keller & Pialli, 1990; Massa et al., 2017; Pertusati et al., 1993).

The character of the widespread broken formations, largely derived from the Palombini shales (e.g., Figures 5a, 5b and 8e) and typical for subduction settings, suggests deformation started when the sediments were poorly lithified and/or saturated in fluids (i.e., in the shallow plate boundary; e.g., Bettelli & Vannucchi, 2003; Vannucchi & Bettelli, 2002). The variable orientation of carbonate veins in the Palombini shales (e.g., Figure 5) further supports the presence of a fluid-saturated tectonic environment. Moreover, in addition to pervasive veining, mélange rocks show reaction rims around sedimentary and mafic blocks indicating extensive availability of fluids for chemical reactions during deformation (e.g., Figures 6e and 6h). The structures preserved within the tectonic lenses of Palombini shales in Norsi, when they are not reworked by the NCC shear zones, are comparable in orientation and deformation style with those recorded by the Palombini shales outside of the NCC in Cavo. In particular, folds with comparable geometry occur in both localities (Figures 5 and 8), showing identical subhorizontal axial planes, tight to isoclinal hinges, and N–S trending axes (stereonet a1 in Figure 5; stereonet a7 in Figure 7). Folding is compatible with deformation within the accretionary prism and this style of folding is well documented in the Palombini shales accreted in the Ligurian prism in the inner and outer Northern Apennines (Bettelli & Vannucchi, 2003; Elter, 1975a; Marroni & Pandolfi, 1996). Finally, the thickness of the NCC, between 30–40 m in Cavo and 500 m in Norsi, and its structure, marked by thick mélange zones and metric shear zones with tectonic slices and cataclastic/foliated fabrics (e.g., Figures 6 and 11), requires an extremely high cumulated strain, which is possible in subduction zones. Indeed, both geophysical studies from currently active subduction channels (e.g., Calahorrano et al., 2008; Collot et al., 2011) and geological studies of fossil subduction channels (e.g., Angiboust et al., 2015; Bachmann, Glodny, et al., 2009; Bachmann, Oncken, et al., 2009; Ujiie & Kimura, 2014) document thick (hundreds of meters to kilometer-scale) zones of intense deformation of oceanic ophiolites and sediments, compatible with the thicknesses we observe on Elba. Finally, the fluid-rich deformation

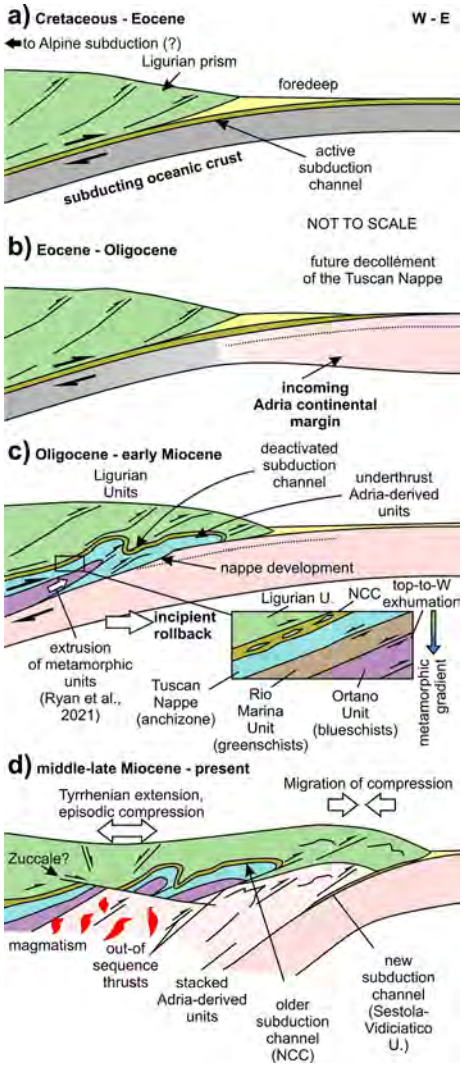

Figure 12. Sketch showing the evolution of the nappe stack from the Cretaceous to present, based on observations from Elba. (a) Cretaceous-Eocene: development of a subduction channel (Norsi-Cavo Complex [NCC]) above an E-verging subduction system. (b) Eocene–Oligocene: arrival of the Adria continental margin in the subduction channel. (c) Oligocene–early Miocene: accretion of continent-derived nappes and deactivation of the oceanic subduction channel. The inset highlights top-to-W extrusion wedge exhumation active in the underlying continental nappes at this stage, producing a normal metamorphic gradient (Ryan et al., 2021). (d) Miocene–present: outward migration of the compressional front of the Apennines, extension, magmatism and out-of-sequence thrusting in the Tyrrhenian Sea. Formation of a new subduction channel (Sestola-Vidiciatico Unit; Vannucchi et al., 2008) at the Apennine front. In this scheme, the ZF is shown as a low-angle normal fault (e.g., Smith et al., 2011), although other authors interpret it as a thrust (e.g., Viola et al., 2018). See text for a detailed commentary.

conditions of the NCC are consistent with the study by Collot et al. (2011) and related papers that show that the subduction channel is a fluid-saturated low-velocity layer. Thus, we suggest that the Norsi-Cavo Complex represents a fossil subduction channel (Figure 13a), likely the internal counterpart of other plate boundary structures recognized in the external part of the belt (i.e., the Sestola-Vidiciatico Unit; Vannucchi et al., 2008).

In Figure 12, we show a conceptual model of the development, evolution, and subsequent deactivation of the NCC subduction channel which shows how this structure might have survived the later tectonic evolution. The NCC developed at the subduction interface (Figure 12a), between the downgoing oceanic plate and the overlying accretionary prism (Ligurian Units). It is unclear how this structure might be related or passes to alpine-verging structures (like Alpine Corsica), but all kinematic indicators in the Elba area are associated with top-to-E deformation, consistent with the W-dipping Apennine subduction, active between the late Cretaceous and the Eocene. When the margin of the Adria microplate entered subduction in the Oligocene (Figure 12b), it caused a change in behavior and deformation style of the system (Figure 12c). During this phase, coherent nappes were accreted from the downgoing Adriatic lithosphere (Subligurian Units and Tuscan Units) with some units experiencing subduction-related blueschist-facies metamorphism (Papeschi et al., 2020; Ryan et al., 2021), while the fossil accretionary prism remained on top of the nappe pile, including the (now) inactive NCC subduction channel. The subduction of continental rocks requires a mature W-dipping subduction before the Oligocene–early Miocene (Rossetti et al., 2002; Ryan et al., 2021). The inactivity of the NCC at this stage on Elba is shown by the lack of continental material (sediments, tectonic slices or blocks) within the NCC and by the presence of later structures—like the Rio Marina antiform, constrained to the middle Miocene and shown in Figure 3b (Massa et al., 2017)—that folded and crosscut the pre-existing NCC. In the latest stages of the Tyrrhenian tectonics (Miocene–present), magmatism was accompanied by pulses of extension and compression (Figure 12d), but the deactivated subduction channel (NCC) survived as a fossil structure, truncated by younger shear zones. The outward propagation of the thrust front and the hinge of the rolling subduction produced a younger subduction channel (Sestola-Vidiciatico Unit) at the front of the Northern Apennines (Vannucchi et al., 2008).

4.2. Conditions of Deformation of the Norsi-Cavo Complex

The Norsi-Cavo Complex consists of very low-grade rocks that recorded deformation at diagenetic to anchizone conditions. According to Pandeli et al. (2001), the metamorphism of the Palombini shales in Cavo does not exceed the high diagenesis/anchizone (illite crystallinity, $\Delta 2\theta = 0.41$–0.51). The ultramafic rocks of Eastern Elba are also low-grade rocks, characterized by lizardite-chrysotile parageneses (Viti & Mellini, 1998). There are no direct temperature and pressure constraints, but overall, illite crystallinity indicates temperatures around ~120°C–200°C. The blueschist-facies parageneses preserved in the underlying continent-derived units on Elba reached $P = 1.5$–1.8 GPa at $T = 320$°C–370°C before 20 Ma (based on phase equilibria modeling and $^{40}Ar/^{39}Ar$ dating; Papeschi et al., 2020; Ryan et al., 2021 and references therein). If we assume that the geothermal gradient did not change substantially from the oceanic subduction to the continental convergence stage and assuming a density of the crust 2.8 g/cm^3, we can estimate a subduction gradient of 6–8°C/km for these rocks. If the Palombini shales were subducted at similar gradients, they might have reached around 15–20 km depth. This depth might be lower if the geothermal gradient was hotter, as it is common

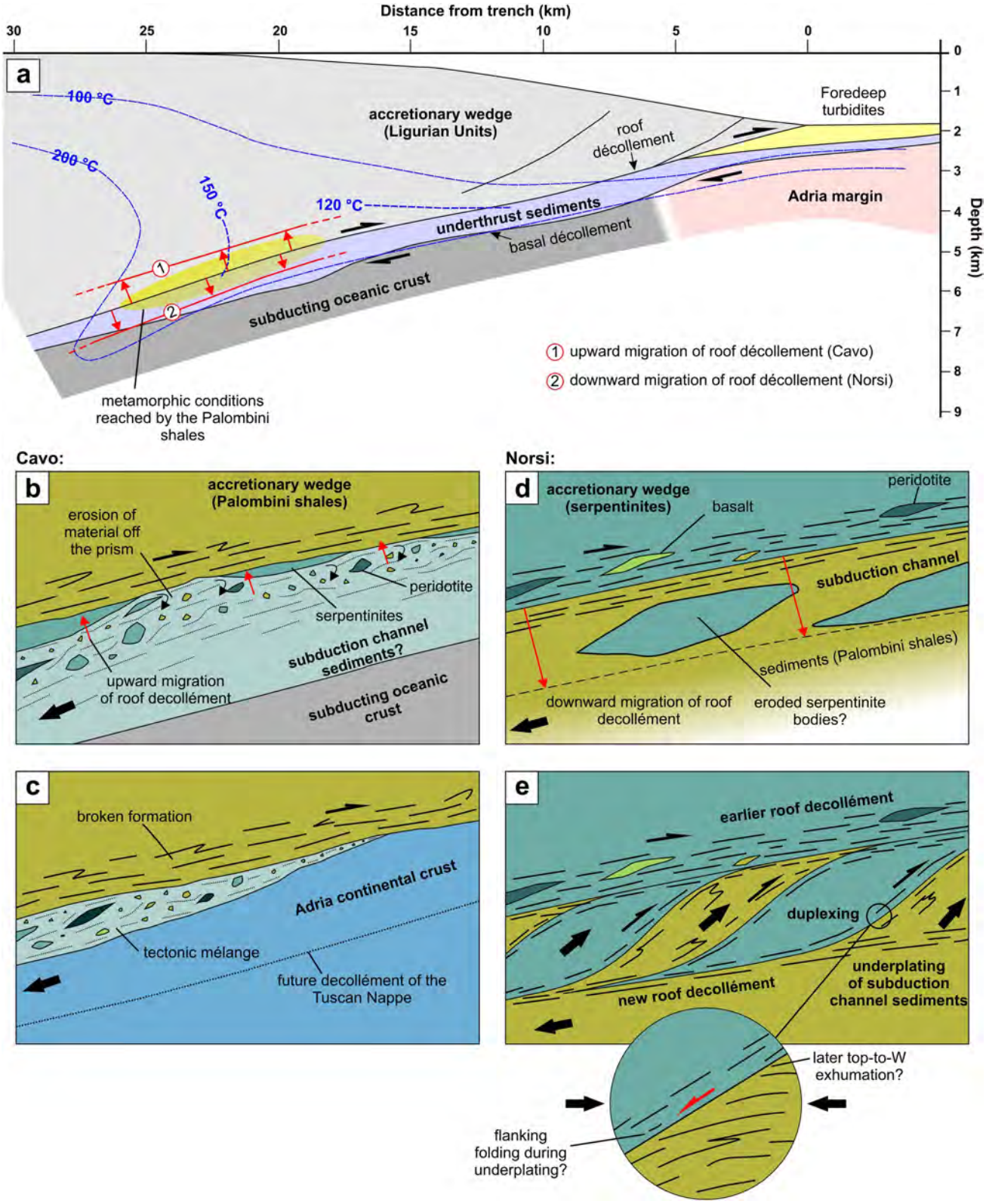
Distance from trench (km)
30
25
20
15
10
5
0
a
100 °C
200 °C
150 °C
120 °C
accretionary wedge
(Ligurian Units)
roof
décollement
Foredeep
turbidites
Adria margin
underthrust sediments
basal décollement
subducting oceanic crust
metamorphic conditions
reached by the Palombini
shales
1 upward migration of roof décollement (Cavo)
2 downward migration of roof décollement (Norsi)
Depth (km)
0
1
2
3
4
5
6
7
8
9
Cavo:
b
accretionary wedge
(Palombini shales)
erosion of
material off
the prism
peridotite
serpentinites
subduction channel
sediments?
upward migration
of roof decollément
subducting oceanic
crust
Norsi:
d
accretionary wedge
(serpentinites)
basalt
peridotite
subduction channel
sediments (Palombini shales)
downward migration of roof
decollément
eroded serpentinite
bodies?
c
broken formation
Adria continental crust
tectonic mélange
future decollément of the
Tuscan Nappe
e
earlier roof decollément
duplexing
new roof decollément
underplating
of subduction
channel sediments
later top-to-W
exhumation?
flanking
folding during
underplating?

Figure 13.

in the early stages of oceanic convergence, or the density of the overlying rocks was higher. We can estimate independently the paleodepth of the observed structures within the subduction channel by applying the model of Vannucchi, Sage, et al. (2012): at shallow depths (T up to 120°C–150°C, up to 5/15 km of burial), the vertical σ_1 produces widespread normal faulting and tensional veins within the subduction channel (see also Collot et al., 2011). On the other hand, at greater depths (>5–15 km and T > 150°C), corresponding to the shallow zone of seismogenesis, the subduction channel consists of a thick shear zone with ductile/cataclastic structures and veins (Vannucchi, Sage, et al., 2012). The situation we describe on Elba is consistent with the latter case. Although more precise *P*/*T* constraints are needed for these rocks, we note that the estimates from the geothermal gradients of blueschist-facies rocks, T estimates from illite crystallinity, and the structural record we observe are consistent with depths close to the shallow zone of seismogenesis (i.e., >5–15 km; Figure 13a). In this sense, the Norsi-Cavo Complex likely represents a deeper portion of the subduction channel compared to the Sestola-Vidiciatico Unit, which mostly deformed at depth <3–5 km (Vannucchi et al., 2008).

4.3. Cavo and Norsi: Two End-Members of Subduction Channel Processes?

The documented subduction channel of Elba is characterized by lenses of oceanic sediments (in large part Palombini shales) within ultramafic rocks. We document two situations with remarkably different tectonic structures and deformation features, although they are characterized by similar top-to-E kinematics: Cavo and Norsi.

Cavo is the only place on the island where the ultramafic rocks that commonly constitute a sequence of several hundred meters at the base of the ophiolitic Ligurian Unit are reduced to a 30–40 m thick serpentinite mélange zone with heterometric blocks of sedimentary rocks and ophiolites (Figure 6). Another situation that is unique to Cavo is that the Palombini shales, which usually constitute the base of the Ligurian Units, here maintain a stratigraphic contact with the older Calpionelle limestones (Figure 3). The mélange in Cavo consists of a serpentine + carbonate-rich matrix with dominant top-to-E kinematics containing blocks of ultramafic rocks, mafic rocks, and abundant fragments of limestone, marl, and shale. These latter sedimentary components come from the overlying Palombini shales. Limestone blocks are surrounded by reaction rims; they typically contain pre-existing tectonic structures, like veins, that are truncated by the mélange foliation (e.g., Figure 6g).

Instead, in Norsi and in most of the island, coherent lenses of Palombini shales occur tectonically intercalated within ultramafic rocks, largely serpentinites, at the base of the Ligurian Unit. As shown in Figures 7 and 10, the contact between the lenses of Palombini shales, the youngest oceanic sediments on Elba, and the ultramafic rocks occurs through meter- to tens of meters-thick shear zones. These shear zones consist of material derived from both the serpentinites/peridotites and the Palombini shales (Figures 10 and 11), and, to a lesser extent, from other lithologies like mafic rocks. We observe a strain gradient in both rock types, marked by ductile deformation and cataclasis of the serpentinites and an intense stratal disruption of the Palombini shales that increases toward the contact between the two lithologies (Figure 8). Serpentinite shear zones, mixed with Palombini-derived material, show constant top-to-E kinematics. Just in one outcrop we observe a top-to-W shear zone at the contact between serpentinites and a lenses of Palombini shales (Figure 8a).

These geological observations imply that the Cavo-Norsi Complex represents a fossil, now exhumed, subduction channel (Cloos & Shreve, 1988a, 1998b)—that is, a subduction boundary shear zone—that is preserved at the base of the Ligurian Units. The subduction channel interpretation also allows us to reconcile the differences observed between Cavo and Norsi (Vannucchi et al., 2012a). The situation observed in Cavo can be considered to be an erosive subduction channel, where the upward migration of the roof décollement has caused the incorporation of material derived from the wedge into the subduction channel (Figures 13b and 13c). This interpretation is based on (a) the relative thinner height of the peridotite/serpentinite sequence compared to the rest of the island, (b) the formation of a tectonic mélange with mixed ophiolitic and sedimentary material, and (c) the tectonically-driven incorporation of material derived from the Palombini shales into the serpentinite mélange.

Figure 13. The proposed subduction channel shear zone on Elba. (a) Schematic model of the fossil Apenninic subduction channel, based on Figure 1 of Vannucchi et al. (2008). and with thermal constraints based on the Costa Rica Margin (Harris & Wang, 2002). The situations we document in Cavo and Norsi are representative, respectively, of (b–c) the upward and (d–e) downward migration of the roof decollément (Vannucchi, Sage, et al., 2012; Vannucchiet, Remitti, et al., 2012). (b) The upward migration of the decollément causes tectonic erosion of material from the wedge and its incorporation in the subduction channel. (c) The Cavo mélange is here interpreted as a remnant of this process. (d) The downward migration of the roof decollément produces accretion of tectonic slices of underplated sediments and serpentinites, likely eroded away from other parts of the wedge, at the base of the accretionary wedge, producing the duplex structure observed at Norsi. See text for further details.

The blocks of Palombini shales likely derive from the extensive exposures of Palombini shales in the nearby hanging wall block. In fact, even though similar tectonic structures (veins, fractures) could have been also formed at the top of the subducting slab, there is no indication of the composition of the original lower plate. At present the footwall block is occupied by the Tuscan Units that reached the subduction zone only in the Oligocene (e.g., Keller & Pialli, 1990), while it appears unlikely that the original footwall also consisted of Palombini shales and not of younger (Cretaceous–Paleogene?) trench sediments. The presence of other components, like blocks of mafic rocks, can be explained either as material eroded (and therefore no longer present) from the overlying prism or locally offscraped from the subducting slab. The process of tectonic erosion could also explain the limited thickness and strong tectonization of serpentinites in Cavo, where they are only 30–40 m thick (vs > 500 m in Norsi), since tectonic erosion is a destructive process that removes material from the wedge. It is likely that only some of this material was preserved there when the Adriatic margin entered the subduction zone, halting tectonic erosion and driving the downward migration of the decollément, to incorporate continent-derived nappes in the early orogenic prism (Figure 13c).

On the other hand, in Norsi the youngest sediments of the oceanic sequence are in direct contact with oceanic mantle rocks (serpentinite and ophicarbonate rocks) right at the base of the ophiolitic unit. This situation is consistent with an accretionary subduction channel, in which the downward migration of the top décollement allowed the accretion/underplating of material from the channel and at the base of the prism. In this model, the top-to-E shear zones observed at the base of the ultramafic rocks and characterized by intense veining and mixing of ultramafic, mafic, and sedimentary material formed at the subduction interface between the base of the Ligurian Units and the subducting Palombini shales (Figures 13d and 13e). As discussed above, the slices of Palombini shales preserve folds and other deformation structures that are comparable to those in the Palombini shales occurring above the subduction channel in Cavo, and typical of the same formation in other outcrops of the Apennine accretionary prism. Indeed, these structures have already been described in the Palombini shales in other parts of the belt and are indicative of folding in a compressive domain (Bettelli & Vannucchi, 2003; Vannucchi & Bettelli, 2002). This structural style differs from the deformation characterizing the plate boundary shear zone outcropping in the outer zone of the Northern Apennines (e.g., Sestola-Vidiciatico), which is represented by bedding-parallel simple shearing and flattening (Vannucchi et al., 2008, Vannucchi, Sage, et al., 2012). This difference in finite strain between the intra-prism and plate boundary deformation style has been noted also in other settings, like Kodiak, the Alps, and Christalls Beach (Bachmann, Oncken, et al., 2009; Bachmann, Glodny, et al., 2009; Fagereng et al., 2010; Fisher & Byrne, 1987).Therefore, we explain the presence of folded lenses of Palombini shales at the base of the serpentinites as the result of incorporation of already deformed material from the upper plate into the subduction channel. Norsi, therefore, has frozen a situation where slices of sediment removed from the upper plate through a process of tectonic erosion have been re-accreted at the top of the subduction channel (Figure 13e), likely at deeper structural levels. It is also possible that the serpentinite slices themselves derived from the erosion of the overlying thick ophiolitic sequence, and that they were entrained in the subduction channel before being re-accreted in Norsi. Indeed, if serpentinites were already present in the subduction channel (Figure 13d), the downward migration of the roof decollément of the subduction channel would have allowed the successive accretion of lenses (horses) of serpentinite and Palombini shales to form a duplex structure (e.g., Raimbourg et al., 2019) (Figure 13e). This process might have occurred several times during the geologic evolution of the Elba subduction channel, with tectonic erosion removing material off some portions of the prism and underplating accreting the eroded material in other segments of the subduction channel. Angiboust et al. (2015) also documented superimposed lenses of material (duplexes) derived from the subduction channel in the western Alps, interpreting them as multiple episodes of accretion during the Alpine subduction. In this scenario, the top-to-W shear zones occurring in the sediments (Figure 13e) could be explained as later exhumation-related features, similar to the top-to-W shear zones described by Ryan et al. (2021) in the nearby blueschist-facies rocks. However, since we do not observe cross-cutting relationships between the top-to-W and the top-to-E shear zones, we prefer to interpret them as the result of compression at the interface between serpentinite and Palombini shales bodies, which resulted in a deflection of the foliation (as large-scale flanking structures; Passchier, 2001).

The scale of the transition between the situations of Norsi and Cavo, although possibly diachronous and documenting different stages of the history of the Ligurian subduction, is on the order of tens of kilometers, consistent with the transitions between accretionary and erosional margins observed in modern subduction zones when trenches experience subduction of topographic highs or incipient collision (e.g., New Britain Trench; Galewsky

& Silver, 1997; Honza et al., 1989; Riker-Coleman et al., 2006). Similar lateral changes in deformation style and composition of mélange blocks and its fabrics have also been observed in Arosa by Bachmann, Oncken, et al. (2009 and Bachmann, Glodny, et al., 2009) and are supported by numerical modeling, showing transient changes between underplating and erosion (Angiboust et al., 2021).

5. Conclusions

Our detailed structural analysis of the Norsi-Cavo Complex, an ensemble of tectonic slices developed at the contact between a fossil oceanic accretionary wedge and underplated continent-derived units documents a fossil—and now exhumed -Alpine subduction channel in the hinterland zone of the Northern Apennines. Field relationships suggest that this subduction channel developed between the Upper Cretaceous and the Oligocene, that is, between the age of the youngest oceanic sediment involved in the Norsi-Cavo Complex and the age of the underlying foredeep deposits of the Northern Apennines. Structures and available metamorphic data indicate that the deformation recorded in this subduction channel is representative of the shallow zone of seismogenesis (5–15 km deep) of a subduction zone. We analyzed in detail two key sites of this subduction channel, showing that it preserves large-scale tectonic structures that may represent an example of (a) tectonic erosion of material from the base of the wedge into the subduction channel and (b) underplating of material into the accretionary wedge from the subduction channel. Future studies, directed toward the high-resolution analysis of the structures preserved on Elba, could help constrain better the dynamics of the Alpine subduction and the mechanisms associated with the subduction process in general.

Data Availability Statement

The data associated with the present study (measurements of geologic structures) is freely available in the repository at the following https://doi.org/10.17632/d64m44ncrh.1.

Acknowledgments
We thank the "brothers" of the Margidore Yacht Club for providing assistance in reaching the coastal outcrops of Norsi by boat. We also thank Giuseppe Nirta for many fruitful and stimulating discussions in the field. This manuscript greatly benefited from the stimulating and constructive reviews of Onno Oncken and Hugues Raimbourg and the editorial work of Jonathan Aitchinson, whom we acknowledge. This work was funded by the JAMSTEC Young Research Fellow funds of S. Papeschi.

References

Abbate, E., Bortolotti, V., Conti, M., Marcucci, M., Principi, G., Passerini, P., & Treves, B. (1986). Apennines and Alps ophiolites and the evolution of the Western Tethys. *Memorie della Societa Geologica Italiana*, *31*, 23–44.

Abers, G. A., van Keken, E., Kneller, E. A., Ferris, A., & Stachnik, J. C. (2006). The thermal structure of subduction zones constrained by seismic imaging: Implications for slab dehydration and wedge flow. *Earth and Planetary Science Letters*, *241*(3–4), 387–397. https://doi.org/10.1016/j.epsl.2005.11.055

Agard, P., Plunder, A., Angiboust, S., Bonnet, G., & Ruh, J. (2018). The subduction plate interface: Rock record and mechanical coupling (from long to short timescales). *Lithos*, *320*, 537–566. https://doi.org/10.1016/j.lithos.2018.09.029

Agard, P., Yamato, P., Jolivet, L., & Burov, E. (2009). Exhumation of oceanic blueschists and eclogites in subduction zones: Timing and mechanisms. *Earth-Science Reviews*, *92*(1–2), 53–79. https://doi.org/10.1016/j.earscirev.2008.11.002

Angiboust, S., Glodny, J., Oncken, O., & Chopin, C. (2014). In search of transient subduction interfaces in the Dent Blanche–Sesia tectonic system (W. Alps). *Lithos*, *205*, 298–321. https://doi.org/10.1016/j.lithos.2014.07.001

Angiboust, S., Kirsch, J., Oncken, O., Glodny, J., Monié, P., & Rybacki, E. (2015). Probing the transition between seismically coupled and decoupled segments along an ancient subduction interface. *Geochemistry, Geophysics, Geosystems*, *16*(6), 1905–1922. https://doi.org/10.1002/2015gc005776

Angiboust, S., Muñoz-Montecinos, J., Cambeses, A., Raimondo, T., Deldicque, D., & Garcia-Casco, A. (2021). Jolts in the Jade factory: A route for subduction fluids and their implications for mantle wedge seismicity. *Earth-Science Reviews*, *220*, 103720. https://doi.org/10.1016/j.earscirev.2021.103720

Aoki, Y., Tamano, T., & Kato, S. (1982). Detailed structure of the Nankai Trough from migrated seismic sections: Convergent margins: Field investigations of margin structure and stratigraphy. *M34: Studies in Continental Margin Geology, AAPG Special Volumes*, *34*, 309–322.

Argnani, A. (2012). Plate motion and the evolution of alpine Corsica and Northern Apennines. *Tectonophysics*, *579*, 207–219. https://doi.org/10.1016/j.tecto.2012.06.010

Audet, P., & Bürgmann, R. (2014). Possible control of subduction zone slow-earthquake periodicity by silica enrichment. *Nature*, *510*(7505), 389–392. https://doi.org/10.1038/nature13391

Ayers, J. (1998). Trace element modeling of aqueous fluid–peridotite interaction in the mantle wedge of subduction zones. *Contributions to Mineralogy and Petrology*, *132*(4), 390–404. https://doi.org/10.1007/s004100050431

Bachmann, R., Glodny, J., Oncken, O., & Seifert, W. (2009). Abandonment of the south Penninic–Austroalpine palaeosubduction zone, Central Alps, and shift from subduction erosion to accretion: Constraints from Rb/Sr geochronology. *Journal of the Geological Society*, *166*(2), 217–231. https://doi.org/10.1144/0016-76492008-024

Bachmann, R., Oncken, O., Glodny, J., Seifert, W., Georgieva, V., & Sudo, M. (2009). Exposed plate interface in the European Alps reveals fabric styles and gradients related to an ancient seismogenic coupling zone. *Journal of Geophysical Research*, *114*(B5), B05402. https://doi.org/10.1029/2008jb005927

Baldacci, F., Elter, P., Giannini, E., Giglia, G., Lazzarotto, A., Nardi, R., & Tongiorgi, M. (1967). Nuove osservazioni sul problema della Falda Toscana e sulla interpretazione dei flysch arenacei tipo "Macigno" dell'Appennino settentrionale. *Memorie della Societa Geologica Italiana*, *6*(2), 213–244.

Bangs, N. L. B., Moore, G. F., Gulick, S. P. S., Pangborn, E. M., Tobin, H. J., Kuramoto, S., & Taira, A. (2009). Broad, weak regions of the Nankai Megathrust and implications for shallow coseismic slip. *Earth and Planetary Science Letters*, *284*(1–2), 44–49. https://doi.org/10.1016/j.epsl.2009.04.026

Barberi, F., Dallan, L., Franzini, M., Giglia, G., Innocenti, F., Marinelli, G., et al. (1967). *Carta geologica dell'Isola d'Elba alla scala 1:25.000*. E.I.R.A.

Barberi, F., Dallan, L., Franzini, M., Giglia, G., Innocenti, F., Marinelli, G., et al. (1969). *Note illustrative della Carta geologica d'Italia alla scala 1:100.000, Foglio 126 (Isola d'Elba)*. Servizio Geologico d'Italia.

Barboni, M., Annen, C., & Schoene, B. (2015). Evaluating the construction and evolution of upper crustal magma reservoirs with coupled U/Pb zircon geochronology and thermal modeling: A case study from the Mt. Capanne pluton (Elba, Italy). *Earth and Planetary Science Letters*, *432*, 436–448. https://doi.org/10.1016/j.epsl.2015.09.043

Bartole, R. (1995). The North Tyrrhenian–northern Apennines post-collisional system: Constraints for a geodynamic model. *Terra Nova*, *7*(1), 7–30. https://doi.org/10.1111/j.1365-3121.1995.tb00664.x

Bebout, G. E., & Penniston-Dorland, S. C. (2016). Fluid and mass transfer at subduction interfaces—The field metamorphic record. *Lithos*, *240*, 228–258. https://doi.org/10.1016/j.lithos.2015.10.007

Bettelli, G., & Vannucchi, P. (2003). Structural style of the offscraped Ligurian oceanic sequences of the Northern Apennines: New hypothesis concerning the development of mélange block-in-matrix fabric. *Journal of Structural Geology*, *25*(3), 371–388. https://doi.org/10.1016/s0191-8141(02)00026-3

Bianco, C. (2020). The Capo Castello shear zone (Eastern Elba Island): Deformation at the contact between Oceanic and continent tectonic Units. *Geosciences*, *10*(9), 361. https://doi.org/10.3390/geosciences10090361

Blanco-Quintero, I. F., García-Casco, A., & Gerya, T. V. (2011). Tectonic blocks in serpentinite mélange (eastern Cuba) reveal large-scale convective flow of the subduction channel. *Geology*, *39*(1), 79–82. https://doi.org/10.1130/g31494.1

Boccaletti, M., Calamita, F., Deiana, G., Gelati, R., Massari, F., Moratti, G., & Lucchi, F. R. (1990). Migrating foredeep-thrust belt systems in the Northern Apennines and Southern Alps. *Palaeogeography, Palaeoclimatology, Palaeoecology*, *77*(1), 3–14. https://doi.org/10.1016/0031-0182(90)90095-o

Boccaletti, M., Elter, P., & Guazzone, G. (1971). Plate tectonic models for the development of the Western Alps and Northern Apennines. *Nature Physical Science*, *234*(49), 108–111. https://doi.org/10.1038/physci234108a0

Bonini, M., Sani, F., Stucchi, E. M., Moratti, G., Benvenuti, M., Menanno, G., & Tanini, C. (2014). Late Miocene shortening of the Northern Apennines back-arc. *Journal of Geodynamics*, *74*, 1–31. https://doi.org/10.1016/j.jog.2013.11.002

Bortolotti, V., Cellai, D., Martin, S., Principi, G., Tartarotti, P., & Vaggelli, G. (1994). Ultramafic rocks from the Eastern Elba Island ophiolites (Tyrrhenian Sea, Italy). *Memorie della Societa Geologica Italiana*, *48*(1), 195–202.

Bortolotti, V., Fazzuoli, M., Pandeli, E., Principi, G., Babbini, A., & Corti, S. (2001). Geology of Central and eastern Elba Island, Italy. *Ofioliti*, *26*(2a), 97–150.

Calahorrano, A., Sallarès, V., Collot, J. Y., Sage, F., & Ranero, C. R. (2008). Nonlinear variations of the physical properties along the southern Ecuador subduction channel: Results from depth-migrated seismic data. *Earth and Planetary Science Letters*, *267*(3–4), 453–467. https://doi.org/10.1016/j.epsl.2007.11.061

Catanzariti, R., Cerrina Feroni, A., Marroni, M., Ottria, G., & Pandolfi, L. (2003). Ophiolites debris in the Aveto unit (Trebbia valley, northern Apennines, Italy): A record of the early Oligocene Apenninic foredeep? *Ofioliti*, *28*, 71.

Cerrina Feroni, A., Plesi, G., Fanelli, G., Leoni, L., & Martinelli, P. (1983). Contributo alla conoscenza dei processi metamorfici di grado molto basso (anchimetamorfismo) a carico della Falda toscana nell'area del ricoprimento apuano. *Bollettino della Societa Geologica Italiana*, *102*(2–3), 269–280.

Ciarapica, G., & Passeri, L. (1994). The Tuscan nappe in Northern Apennines: Data, doubts, hypotheses. *Memorie della Societa Geologica Italiana*, *48*(1), 7–22.

Clift, P. D., & Vannucchi, P. (2004). Controls on tectonic accretion versus erosion in subduction zones: Implications for the origin and recycling of the continental crust. *Reviews of Geophysics*, *42*(2), RG2001. https://doi.org/10.1029/2003rg000127

Clift, P. D., Vannucchi, P., & Morgan, J. P. (2009). Crustal redistribution, crust–mantle recycling and Phanerozoic evolution of the continental crust. *Earth-Science Reviews*, *97*(1–4), 80–104. https://doi.org/10.1016/j.earscirev.2009.10.003

Cloos, M., & Shreve, R. L. (1988a). Subduction-channel model of prism accretion, melange formation, sediment subduction, and subduction erosion at convergent plate margins: 1. Background and description. *Pure and Applied Geophysics*, *128*(3), 455–500. https://doi.org/10.1007/bf00874548

Cloos, M., & Shreve, R. L. (1988b). Subduction-channel model of prism accretion, melange formation, sediment subduction, and subduction erosion at convergent plate margins: 2. Implications and discussion. *Pure and Applied Geophysics*, *128*(3), 501–545. https://doi.org/10.1007/bf00874549

Collettini, C., & Holdsworth, R. E. (2004). Fault zone weakening and character of slip along low-angle normal faults: Insights from the Zuccale Fault, Elba, Italy. *Journal of the Geological Society*, *161*(6), 1039–1051. https://doi.org/10.1144/0016-764903-179

Collot, J. Y., Ribodetti, A., Agudelo, W., & Sage, F. (2011). The south Ecuador subduction channel: Evidence for a dynamic mega-shear zone from 2D fine-scale seismic reflection imaging and implications for material transfer. *Journal of Geophysical Research*, *116*(B11), B11102. https://doi.org/10.1029/2011jb008429

Conti, P., Cornamusini, G., & Carmignani, L. (2020). An outline of the geology of the northern Apennines (Italy), with geological map at 1:250,000 scale. *Italian Journal of Geosciences*, *139*(2), 149–194. https://doi.org/10.3301/ijg.2019.25

Coward, M., & Dietrich, D. (1989). Alpine tectonics—An overview. *Geological Society, London, Special Publications*, *45*(1), 1–29. https://doi.org/10.1144/gsl.sp.1989.045.01.01

Decandia, F. A., & Lazzarotto, A. (1980). Le unità tettoniche del Monte Argentario (Toscana meridionale). *Memorie della Societa Geologica Italiana*, *21*, 385–393.

Deschamps, Y., Dagallier, G., Macaudier, J., Marignac, C., Maine, B., & Saupé, F. (1983). Le gisement de pyritehématite de Valle giove (Rio Marina, Ile d'Elbe, italie). Contribution à la connaissance des gisements de toscane-I. Partie 1. *Schweizerische Mineralogische und Petrographische Mitteilungen*, *63*, 149–165.

Dini, A., Innocenti, F., Rocchi, S., Tonarini, S., & Westerman, D. S. (2002). The magmatic evolution of the late Miocene laccolith–pluton–dyke granitic complex of Elba Island, Italy. *Geological Magazine*, *139*(3), 257–279. https://doi.org/10.1017/s0016756802006556

Duranti, S., Palmeri, R., Pertusati, C., & Ricci, C. A. (1992). Geological evolution and metamorphic petrology of the basal sequences of eastern Elba (complex II). *Acta Vulcanologica*, *2*, 213–229.

Elter, F. M., & Pandeli, E. (2001). Structural evolution of anchi-/epimetamorphic units of Central and Eastern Elba (Ortano, Acquadolce, Monticiano-Roccastrada and Grassera Units). *Ofioliti*, *26*(2a), 219–228.

Elter, G., Elter, P., Sturani, C., & Weidmann, M. (1966). Sur la prolongation du domaine ligure de l'Apennin dans le Montferrat et les Alpes et sur l'origine de la nappe de la Simme sl des Préalpes romandes et chablaisiennes. *Archives des Sciences*, *176*, 279–377.

Elter, P. (1975a). Introduction à la géologie de l'Apennin septentrional. *Bulletin de la Societe Geologique de France*, *XVII*(6), 956–962. https://doi.org/10.2113/gssgfbull.s7-xvii.6.956

Elter, P. (1975b). L'ensemble ligure. *Bullettin dé la Société Géologique de France*, *17*(6), 984–997. https://doi.org/10.2113/gssgfbull.s7-xvii.6.984

Elter, P., Catanzariti, R., Ghiselli, F., Marroni, M., Molli, G., Ottria, G., & Pandolfi, L. (1999). L'unità Aveto (Appennino settentrionale): Caratteristiche litostratigrafiche, biostratigrafia, petrografia delle areniti ed assetto strutturale. *Bollettino della Societa Geologica Italiana*, *118*, 41–64.

Elter, P., Gratziu, C., & Labesse, B. (1964). Sul significato dell'esistenza di una unità tettonica alloctona costituita da formazioni terziarie nell'Appennino settentrionale. *Bollettino della Societa Geologica Italiana*, *83*(2), 373–394.

Elter, P., & Marroni, M. (1991). Le Unità Liguri dell'Appennino settentrionale: Sintesi dei dati e nuove interpretazioni. *Memorie Descrittive della Carta Geologica d'Italia*, *46*, 121–138.

Faccenna, C., Becker, T. W., Auer, L., Billi, A., Boschi, L., Brun, J. P., et al. (2014). Mantle dynamics in the Mediterranean. *Reviews of Geophysics*, *52*(3), 283–332. https://doi.org/10.1002/2013rg000444

Faccenna, C., Davy, P., Brun, J. P., Funiciello, R., Giardini, D., Mattei, M., & Nalpas, T. (1996). The dynamics of back-arc extension: An experimental approach to the opening of the Tyrrhenian Sea. *Geophysical Journal International*, *126*(3), 781–795. https://doi.org/10.1111/j.1365-246x.1996.tb04702.x

Faccenna, C., Funiciello, F., Giardini, D., & Lucente, P. (2001). Episodic back-arc extension during restricted mantle convection in the Central Mediterranean. *Earth and Planetary Science Letters*, *187*(1–2), 105–116. https://doi.org/10.1016/s0012-821x(01)00280-1

Fagereng, Å. (2011). Geology of the seismogenic subduction thrust interface. *Geological Society, London, Special Publications*, *359*(1), 55–76. https://doi.org/10.1144/sp359.4

Fagereng, Å., Remitti, F., & Sibson, R. H. (2010). Shear veins observed within anisotropic fabric at high angles to the maximum compressive stress. *Nature Geoscience*, *3*(7), 482–485. https://doi.org/10.1038/ngeo898

Federico, L., Crispini, L., Scambelluri, M., & Capponi, G. (2007). Ophiolite mélange zone records exhumation in a fossil subduction channel. *Geology*, *35*(6), 499–502. https://doi.org/10.1130/g23190a.1

Fisher, D., & Byrne, T. (1987). Structural evolution of underthrusted sediments, Kodiak Islands, Alaska. *Tectonics*, *6*(6), 775–793. https://doi.org/10.1029/tc006i006p00775

Fisher, D. M., & Brantley, S. L. (2014). The role of silica redistribution in the evolution of slip instabilities along subduction interfaces: Constraints from the Kodiak accretionary complex, Alaska. *Journal of Structural Geology*, *69*, 395–414. https://doi.org/10.1016/j.jsg.2014.03.010

Franceschelli, M., Leoni, L., Memmi, I., & Puxeddu, M. (1986). Regional distribution of Al-silicates and metamorphic zonation in the low-grade Verrucano metasediments from the northern Apennines, Italy. *Journal of Metamorphic Geology*, *4*(3), 309–321. https://doi.org/10.1111/j.1525-1314.1986.tb00353.x

Frassi, C., Musumeci, G., Zucali, M., Mazzarini, F., Rebay, G., & Langone, A. (2017). The Cotoncello shear zone (Elba Island, Italy): The deep root of a fossil oceanic detachment fault in the Ligurian ophiolites. *Lithos*, *278*, 445–463. https://doi.org/10.1016/j.lithos.2017.02.015

Gagnevin, D., Daly, J. S., Horstwood, M. S. A., & Whitehouse, M. J. (2011). In-situ zircon U–Pb, oxygen and hafnium isotopic evidence for magma mixing and mantle metasomatism in the Tuscan Magmatic Province, Italy. *Earth and Planetary Science Letters*, *305*(1–2), 45–56. https://doi.org/10.1016/j.epsl.2011.02.039

Galewsky, J., & Silver, E. A. (1997). Tectonic controls on facies transitions in an oblique collision: The western Solomon Sea, Papua New Guinea. *The Geological Society of America Bulletin*, *109*(10), 1266–1278. https://doi.org/10.1130/0016-7606(1997)109<1266:tcofti>2.3.co;2

Gao, X., & Wang, K. (2017). Rheological separation of the megathrust seismogenic zone and episodic tremor and slip. *Nature*, *543*(7645), 416–419. https://doi.org/10.1038/nature21389

Gerya, T. V., Stöckhert, B., & Perchuk, A. L. (2002). Exhumation of high-pressure metamorphic rocks in a subduction channel: A numerical simulation. *Tectonics*, *21*(6), 6–1. https://doi.org/10.1029/2002tc001406

Guillot, S., Hattori, K., Agard, P., Schwartz, S., & Vidal, O. (2009). Exhumation processes in oceanic and continental subduction contexts: A review. In S. Lallemand, & F. Funiciello (Eds.), *Subduction zone Geodynamics* (pp. 175–205). Springer-Verlag Berlin Heidelberg. https://doi.org/10.1007/978-3-540-87974-9

Guillot, S., Schwartz, S., Hattori, K., Auzende, A., & Lardeaux, J. (2004). The Monviso ophiolitic Massif (Western Alps), a section through a serpentinite subduction channel. *Journal of the Virtual Explorer*, *16*, 17. https://doi.org/10.3809/jvirtex.2004.00099

Harris, R. N., & Wang, K. (2002). Thermal models of the middle America trench at the Nicoya Peninsula, Costa Rica. *Geophysical Research Letters*, *29*(21), 6–1. https://doi.org/10.1029/2002gl015406

Honza, E., Miyazaki, T., & Lock, J. (1989). Subduction erosion and accretion in the Solomon Sea region. *Tectonophysics*, *160*(1–4), 49–62. https://doi.org/10.1016/0040-1951(89)90383-1

Ide, S., Beroza, G. C., Shelly, D. R., & Uchide, T. (2007). A scaling law for slow earthquakes. *Nature*, *447*(7140), 76–79. https://doi.org/10.1038/nature05780

Ioannidi, P. I., Angiboust, S., Oncken, O., Agard, P., Glodny, J., & Sudo, M. (2020). Deformation along the roof of a fossil subduction interface in the transition zone below seismogenic coupling: The Austroalpine case and new insights from the Malenco Massif (Central Alps). *Geosphere*, *16*(2), 510–532. https://doi.org/10.1130/ges02149.1

Jacobs, J., Paoli, G., Rocchi, S., Ksienzyk, A. K., Sirevaag, H., & Elburg, M. A. (2018). Alps to Apennines zircon roller coaster along the Adria microplate margin. *Scientific Reports*, *8*(1), 1–8. https://doi.org/10.1038/s41598-018-20979-w

Jolivet, L., Arbaret, L., Le Pourhiet, L., Cheval-Garabedian, F., Roche, V., Rabillard, A., & Labrousse, L. (2021). Interactions of plutons and detachments: A comparison of Aegean and Tyrrhenian granitoids. *Solid Earth*, *12*(6), 1357–1388. https://doi.org/10.5194/se-12-1357-2021

Jolivet, L., Faccenna, C., Goffé, B., Mattei, M., Rossetti, F., Brunet, C., et al. (1998). Midcrustal shear zones in postorogenic extension: Example from the northern Tyrrhenian Sea. *Journal of Geophysical Research*, *103*(B6), 12123–12160. https://doi.org/10.1029/97jb03616

Keller, J. V. A., & Coward, M. P. (1996). The structure and evolution of the northern Tyrrhenian Sea. *Geological Magazine*, *133*(1), 1–16. https://doi.org/10.1017/s0016756800007214

Keller, J. V. A., & Pialli, G. (1990). Tectonics of the island of Elba: A reappraisal. *Bollettino della Societa Geologica Italiana*, *109*(2), 413–425.

Kimura, G., Yamaguchi, A., Hojo, M., Kitamura, Y., Kameda, J., Ujiie, K., et al. (2012). Tectonic mélange as fault rock of subduction plate boundary. *Tectonophysics*, *568*, 25–38. https://doi.org/10.1016/j.tecto.2011.08.025

Kimura, H., Takeda, T., Obara, K., & Kasahara, K. (2010). Seismic evidence for active underplating below the megathrust earthquake zone in Japan. *Science*, *329*(5988), 210–212. https://doi.org/10.1126/science.1187115

Kitamura, Y., Sato, K., Ikesawa, E., Ikehara-Ohmori, K., Kimura, G., Kondo, H., et al. (2005). Mélange and its seismogenic roof décollement: A plate boundary fault rock in the subduction zone—An example from the Shimanto Belt, Japan. *Tectonics*, *24*(5). https://doi.org/10.1029/2004tc001635

Kligfield, R. (1979). The Northern Apennines as a collisional orogen. *American Journal of Science*, *279*(6), 676–691. https://doi.org/10.2475/ajs.279.6.676

Kotowski, A. J., & Behr, W. M. (2019). Length scales and types of heterogeneities along the deep subduction interface: Insights from exhumed rocks on Syros Island, Greece. *Geosphere*, *15*(4), 1038–1065. https://doi.org/10.1130/ges02037.1

Lagabrielle, Y., & Cannat, M. (1990). Alpine Jurassic ophiolites resemble the modern central Atlantic basement. *Geology*, *18*(4), 319–322. https://doi.org/10.1130/0091-7613(1990)018<0319:ajortm>2.3.co;2

Le Breton, E., Brune, S., Ustaszewski, K., Zahirovic, S., Seton, M., & Müller, R. D. (2021). Kinematics and extent of the Piemont–Liguria basin–implications for subduction processes in the Alps. *Solid Earth*, *12*(4), 885–913. https://doi.org/10.5194/se-12-885-2021

Le Breton, E., Handy, M. R., Molli, G., & Ustaszewski, K. (2017). Post-20 Ma motion of the Adriatic Plate: New constraints from surrounding orogens and implications for crust-mantle decoupling. *Tectonics*, *36*(12), 3135–3154. https://doi.org/10.1002/2016tc004443

Locatelli, M., Verlaguet, A., Agard, P., Pettke, T., & Federico, L. (2019). Fluid pulses during stepwise brecciation at intermediate subduction depths (Monviso eclogites, W. Alps): First internally then externally sourced. *Geochemistry, Geophysics, Geosystems*, *20*(11), 5285–5318. https://doi.org/10.1029/2019gc008549

Malinverno, A., & Ryan, W. B. (1986). Extension in the Tyrrhenian Sea and shortening in the Apennines as result of arc migration driven by sinking of the lithosphere. *Tectonics*, *5*(2), 227–245. https://doi.org/10.1029/tc005i002p00227

Marroni, M., Meneghini, F., & Pandolfi, L. (2010). Anatomy of the Ligure-Piemontese subduction system: Evidence from Late Cretaceous–middle Eocene convergent margin deposits in the northern Apennines, Italy. *International Geology Review*, *52*(10–12), 1160–1192. https://doi.org/10.1080/00206810903545493

Marroni, M., Meneghini, F., & Pandolfi, L. (2017). A revised subduction inception model to explain the Late Cretaceous, double-vergent orogen in the precollisional Western Tethys: Evidence from the Northern Apennines. *Tectonics*, *36*(10), 2227–2249. https://doi.org/10.1002/2017tc004627

Marroni, M., & Pandolfi, L. (1996). The deformation history of an accreted ophiolite sequence: The Internal Liguride units (Northern Apennines, Italy). *Geodinamica Acta*, *9*(1), 13–29. https://doi.org/10.1080/09853111.1996.11417260

Marroni, M., & Pandolfi, L. (2007). The architecture of an incipient oceanic basin: A tentative reconstruction of the Jurassic Liguria-Piemonte basin along the northern Apennines–Alpine Corsica transect. *International Journal of Earth Sciences*, *96*(6), 1059–1078. https://doi.org/10.1007/s00531-006-0163-x

Maruyama, S., Liou, J. G., & Terabayashi, M. (1996). Blueschists and eclogites of the world and their exhumation. *International Geology Review*, *38*(6), 485–594. https://doi.org/10.1080/00206819709465347

Massa, G., Musumeci, G., Mazzarini, F., & Pieruccioni, D. (2017). Coexistence of contractional and extensional tectonics during the northern Apennines orogeny: The late Miocene out-of-sequence thrust in the Elba Island nappe stack. *Geological Journal*, *52*(3), 353–368. https://doi.org/10.1002/gj.2761

Mauffret, A., Contrucci, I., & Brunet, C. (1999). Structural evolution of the northern Tyrrhenian Sea from new seismic data. *Marine and Petroleum Geology*, *16*(5), 381–407. https://doi.org/10.1016/s0264-8172(99)00004-5

Meneghini, F., & Moore, J. C. (2007). Deformation and hydrofracture in a subduction thrust at seismogenic depths: The Rodeo Cove thrust zone, Marin Headlands, California. *The Geological Society of America Bulletin*, *119*(1–2), 174–183. https://doi.org/10.1130/b25807.1

Moeller, S., Grevemeyer, I., Ranero, C. R., Berndt, C., Klaeschen, D., Sallarès, V., et al. (2013). Early-stage rifting of the northern Tyrrhenian Sea Basin: Results from a combined wide-angle and multichannel seismic study. *Geochemistry, Geophysics, Geosystems*, *14*(8), 3032–3052. https://doi.org/10.1002/ggge.20180

Moeller, S., Grevemeyer, I., Ranero, C. R., Berndt, C., Klaeschen, D., Sallarès, V., et al. (2014). Crustal thinning in the northern Tyrrhenian Rift: Insights from multichannel and wide-angle seismic data across the basin. *Journal of Geophysical Research: Solid Earth*, *119*(3), 1655–1677. https://doi.org/10.1002/2013jb010431

Molli, G. (2008). Northern Apennine–Corsica orogenic system: An updated overview. *Geological Society, London, Special Publications*, *298*(1), 413–442. https://doi.org/10.1144/sp298.19

Molli, G., Carlini, M., Vescovi, P., Artoni, A., Balsamo, F., Camurri, F., et al. (2018). Neogene 3-D structural architecture of the North-west Apennines: The role of the low-angle normal faults and basement thrusts. *Tectonics*, *37*(7), 2165–2196. https://doi.org/10.1029/2018tc005057

Musumeci, G., Mazzarini, F., & Cruden, A. R. (2015). The Zuccale Fault, Elba Island, Italy: A new perspective from fault architecture. *Tectonics*, *34*(6), 1195–1218. https://doi.org/10.1002/2014tc003809

Musumeci, G., Mazzarini, F., Tiepolo, M., & Di Vincenzo, G. (2011). U-Pb and ^{40}Ar-^{39}Ar geochronology of palaeozoic units in the northern Apennines: Determining protolith age and alpine evolution using the Calamita Schist and Ortano Porphyroid. *Geological Journal*, *46*(4), 288–310. https://doi.org/10.1002/gj.1266

Musumeci, G., & Vaselli, L. (2012). Neogene deformation and granite emplacement in the metamorphic units of northern Apennines (Italy): Insights from mylonitic marbles in the Porto Azzurro pluton contact aureole (Elba Island). *Geosphere*, *8*(2), 470–490. https://doi.org/10.1130/ges00665.1

Nirta, G., Pandeli, E., Principi, G., Bertini, G., & Cipriani, N. (2005). The Ligurian units of southern Tuscany. *Bollettino della Società Geologica Italiana, Volume Speciale*, *3*, 29–54.

Obara, K. (2002). Nonvolcanic deep tremor associated with subduction in southwest Japan. *Science*, *296*(5573), 1679–1681. https://doi.org/10.1126/science.1070378

Obara, K., & Kato, A. (2016). Connecting slow earthquakes to huge earthquakes. *Science*, *353*(6296), 253–257. https://doi.org/10.1126/science.aaf1512

Okamoto, A., Oyanagi, R., Yoshida, K., Uno, M., Shimizu, H., & Satish-Kumar, M. (2021). Rupture of wet mantle wedge by self-promoting carbonation. *Communications Earth & Environment*, *2*(1), 1–10. https://doi.org/10.1038/s43247-021-00224-5

Pandeli, E., Corti, S., Franceschelli, M., & Pecchioni, E. (2001). The varicoloured slates of the Gràssera Unit (Central-Eastern Elba, Tuscany): Petrographical-mineralogical data and comparisons with other Tuscan and Ligurian-Piedmontese units. *Ofioliti*, *26*(2a), 197–206.

Papeschi, S., & Musumeci, G. (2019). Fluid-assisted strain localization in quartz at the brittle/ductile transition. *Geochemistry, Geophysics, Geosystems*, *20*(6), 3044–3064. https://doi.org/10.1029/2019gc008270

Papeschi, S., Musumeci, G., Massonne, H. J., Bartoli, O., & Cesare, B. (2019). Partial melting and strain localization in metapelites at very low-pressure conditions: The northern Apennines magmatic arc on the Island of Elba, Italy. *Lithos*, *350*, 105230. https://doi.org/10.1016/j.lithos.2019.105230

Papeschi, S., Musumeci, G., Massonne, H. J., Mazzarini, F., Ryan, E. J., & Viola, G. (2020). High-P (P = 1.5–1.8 GPa) blueschist from Elba: Implications for underthrusting and exhumation of continental units in the northern Apennines. *Journal of Metamorphic Geology*, *38*(5), 495–525. https://doi.org/10.1111/jmg.12530

Papeschi, S., Musumeci, G., & Mazzarini, F. (2017). Heterogeneous brittle-ductile deformation at shallow crustal levels under high thermal conditions: The case of a synkinematic contact aureole in the inner northern Apennines, southeastern Elba Island, Italy. *Tectonophysics*, *717*, 547–564. https://doi.org/10.1016/j.tecto.2017.08.020

Papeschi, S., Musumeci, G., & Mazzarini, F. (2018). Evolution of shear zones through the brittle-ductile transition: The Calamita Schists (Elba Island, Italy). *Journal of Structural Geology*, *113*, 100–114. https://doi.org/10.1016/j.jsg.2018.05.023

Papeschi, S., Pontesilli, A., Romano, C., Rossetti, F., & Theye, T. (2022). Alpine subduction zone metamorphism in the Palaeozoic successions of the Monti Romani (northern Apennines, Italy). *Journal of Metamorphic Geology*, *40*(5), 1–35. https://doi.org/10.1111/jmg.12650

Papeschi, S., Ryan, E., Musumeci, G., Mazzarini, F., Garofalo, P. S., & Viola, G. (2021). Geology of the northern Apennines nappe stack on eastern Elba (Italy): New insights on the Neogene orogenic evolution of the northern Tyrrhenian Sea. *Journal of Maps*, *17*(2), 519–532. https://doi.org/10.1080/17445647.2021.1972854

Passchier, C. W. (2001). Flanking structures. *Journal of Structural Geology*, *23*(6–7), 951–962. https://doi.org/10.1016/s0191-8141(00)00166-8

Patacca, E., Sartori, R., & Scandone, P. (1990). Tyrrhenian basin and apenninic arcs: Kinematic relations since late Tortonian times. *Memorie della Societa Geologica Italiana*, *45*, 425–451.

Peacock, S. A. (1990). Fluid processes in subduction zones. *Science*, *248*(4953), 329–337. https://doi.org/10.1126/science.248.4953.329

Pearce, J. A., Alabaster, T., Shelton, A. W., & Searle, M. P. (1981). The Oman ophiolite as a Cretaceous arc-basin complex: Evidence and implications. *Philosophical Transactions of the Royal Society of London—Series A: Mathematical and Physical Sciences*, *300*(1454), 299–317.

Peng, Z., & Gomberg, J. (2010). An integrated perspective of the continuum between earthquakes and slow-slip phenomena. *Nature Geoscience*, *3*(9), 599–607. https://doi.org/10.1038/ngeo940

Perrin, M. (1969). Contribution à l'étude de la Nappe ophiolitifère dans l'Elbe orientale. *Atti della Società Toscana di Scienze Naturali, Memorie, Serie A*, *76*, 45–87.

Perrin, M. (1975). L'Ile d'Elbe et la limite Alpes-Apennin: Données sur la structure géologique et l'évolution tectogénétique de l'Elbe alpine et de l'Elbe apennine. *Bollettino della Societa Geologica Italiana*, *94*, 1929–1955.

Perrin, M., & Neumann, M. (1970). Présence, au NE de l'Ile d'Elbe d'une série de type "scisti policromi" à faune maestrichtienne. *Comptes Rendus de l'Académie de Sciences, Series D*, *270*, 2260–2263.

Pertusati, C., Raggi, G., Ricci, C. A., Duranti, S., & Palmeri, R. (1993). Evoluzione post-collisionale dell'Elba centro-orientale. *Memorie della Societa Geologica Italiana*, *49*, 297–312.

Plunder, A., Agard, P., Chopin, C., Pourteau, A., & Okay, A. I. (2015). Accretion, underplating and exhumation along a subduction interface: From subduction initiation to continental subduction (Tavşanlı zone, W. Turkey). *Lithos*, *226*, 233–254. https://doi.org/10.1016/j.lithos.2015.01.007

Principi, G., Bortolotti, V., Pandeli, E., Fanucci, F., Benvenuti, M., Chiari, M., et al. (2015). *Note illustrative della Carta geologica d'Italia alla scala 1:50.000. Foglio 316, 317, 328, 329 (Isola d'Elba)*. Servizio Geologico d'Italia.

Principi, G., & Treves, B. (1984). Il sistema Corso-Appenninico come prisma di accrezione. Riflessi sul problema generale del limite Alpi-Appennini. *Memorie della Societa Geologica Italiana*, *28*, 549–576.

Raimbourg, H., Famin, V., Palazzin, G., Yamaguchi, A., Augier, R., Kitamura, Y., & Sakaguchi, A. (2019). Distributed deformation along the subduction plate interface: The role of tectonic mélanges. *Lithos*, *334*, 69–87. https://doi.org/10.1016/j.lithos.2019.01.033

Ramsay, J. G., & Huber, M. I. (1987). *The techniques of modern structural geology*. Academic Press.

Remitti, F., Bettelli, G., & Vannucchi, P. (2007). Internal structure and tectonic evolution of an underthrust tectonic mélange: The Sestola-Vidiciatico tectonic unit of the Northern Apennines, Italy. *Geodinamica Acta*, *20*(1–2), 37–51. https://doi.org/10.3166/ga.20.37-51

Remitti, F., Vannucchi, P., Bettelli, G., Fantoni, L., Panini, F., & Vescovi, P. (2011). Tectonic and sedimentary evolution of the frontal part of an ancient subduction complex at the transition from accretion to erosion: The case of the Ligurian wedge of the Northern Apennines, Italy. *Bulletin*, *123*(1–2), 51–70. https://doi.org/10.1130/b30065.1

Reutter, K. J., & Spohn, A. (1982). The position of the West-Elba ophiolites within the tectonic framework of the Apennines. *Ofioliti*, *7*(2–3), 467–478.

Ricci Lucchi, F. (1986). The Oligocene to Recent foreland basins of the northern Apennines. In A. Allen, & P. Homewood (Eds.) (Vol. 8, pp. 105–139). *Foreland basins. International association of sedimentologists special publications*. Blackwell Scientific Publications.

Riker-Coleman, K. E., Gallup, C. D., Wallace, L. M., Webster, J. M., Cheng, H., & Edwards, R. L. (2006). Evidence of Holocene uplift in east new Britain, Papua New Guinea. *Geophysical Research Letters*, *33*(18). https://doi.org/10.1029/2006gl026596

Ring, U., Pantazides, H., Glodny, J., & Skelton, A. (2020). Forced return flow deep in the subduction channel, Syros, Greece. *Tectonics*, *39*(1), e2019TC005768. https://doi.org/10.1029/2019tc005768

Rogers, G., & Dragert, H. (2003). Episodic tremor and slip on the Cascadia subduction zone: The chatter of silent slip. *Science*, *300*(5627), 1942–1943. https://doi.org/10.1126/science.1084783

Rossetti, F., Faccenna, C., Jolivet, L., Funiciello, R., Goffé, B., Tecce, F., et al. (2001). Structural signature and exhumation P-T-t path of the Gorgona blueschist sequence (Tuscan Archipelago, Italy). *Ofioliti*, *26*(2a), 175–186.

Rossetti, F., Faccenna, C., Jolivet, L., Goffé, B., & Funiciello, R. (2002). Structural signature and exhumation P-T-t paths of the blueschist units exposed in the interior of the Northern Apennine chain, tectonic implications. *Bollettino della Societa Geologica Italiana*, *121*(1), 829–842.

Rossetti, F., Tecce, F., Billi, A., & Brilli, M. (2007). Patterns of fluid flow in the contact aureole of the Late Miocene Monte Capanne pluton (Elba Island, Italy): The role of structures and rheology. *Contributions to Mineralogy and Petrology*, *153*(6), 743–760. https://doi.org/10.1007/s00410-006-0175-3

Rowe, C. D., Meneghini, F., & Moore, J. C. (2011). Textural record of the seismic cycle: Strain-rate variation in an ancient subduction thrust. *Geological Society, London, Special Publications*, *359*(1), 77–95. https://doi.org/10.1144/sp359.5

Rowe, C. D., Moore, J. C., & Remitti, F., & IODP Expedition 343/343T Scientists. (2013). The thickness of subduction plate boundary faults from the seafloor into the seismogenic zone. *Geology*, *41*(9), 991–994. https://doi.org/10.1130/g34556.1

Ryan, E., Papeschi, S., Viola, G., Musumeci, G., Mazzarini, F., Torgersen, E., et al. (2021). Syn-orogenic exhumation of high-P units by upward extrusion in an accretionary wedge: Insights from the Eastern Elba nappe stack (northern Apennines, Italy). *Tectonics*, *40*(5), e2020TC006348. https://doi.org/10.1029/2020tc006348

Sage, F., Collot, J. Y., & Ranero, C. R. (2006). Interplate patchiness and subduction-erosion mechanisms: Evidence from depth-migrated seismic images at the central Ecuador convergent margin. *Geology*, *34*(12), 997–1000. https://doi.org/10.1130/g22790a.1

Schwartz, S., Allemand, P., & Guillot, S. (2001). Numerical model of the effect of serpentinites on the exhumation of eclogitic rocks: Insights from the Monviso ophiolitic massif (Western Alps). *Tectonophysics*, *342*(1–2), 193–206. https://doi.org/10.1016/s0040-1951(01)00162-7

Schwartz, S. Y., & Rokosky, J. M. (2007). Slow slip events and seismic tremor at circum-Pacific subduction zones. *Reviews of Geophysics*, *45*(3), 2006RG000208. https://doi.org/10.1029/2006rg000208

Searle, M., & Cox, J. (1999). Tectonic setting, origin, and obduction of the Oman ophiolite. *The Geological Society of America Bulletin*, *111*(1), 104–122. https://doi.org/10.1130/0016-7606(1999)111<0104:tsoaoo>2.3.co;2

Serri, G., Innocenti, F., & Manetti, P. (1993). Geochemical and petrological evidence of the subduction of delaminated Adriatic continental lithosphere in the genesis of the Neogene-Quaternary magmatism of central Italy. *Tectonophysics*, *223*(1–2), 117–147. https://doi.org/10.1016/0040-1951(93)90161-c

Shelly, D. R., Beroza, G. C., Ide, S., & Nakamula, S. (2006). Low-frequency earthquakes in Shikoku, Japan, and their relationship to episodic tremor and slip. *Nature*, *442*(7099), 188–191. https://doi.org/10.1038/nature04931

Shreve, R. L., & Cloos, M. (1986). Dynamics of sediment subduction, melange formation, and prism accretion. *Journal of Geophysical Research*, *91*(B10), 10229–10245. https://doi.org/10.1029/jb091ib10p10229

Smith, S. A. F., Holdsworth, R. E., & Collettini, C. (2011). Interactions between low-angle normal faults and plutonism in the upper crust: Insights from the Island of Elba, Italy. *The Geological Society of America Bulletin*, *123*(1–2), 329–346. https://doi.org/10.1130/b30200.1

Taetz, S., John, T., Bröcker, M., Spandler, C., & Stracke, A. (2018). Fast intraslab fluid-flow events linked to pulses of high pore fluid pressure at the subducted plate interface. *Earth and Planetary Science Letters*, *482*, 33–43. https://doi.org/10.1016/j.epsl.2017.10.044

Tartarotti, P., & Vaggelli, G. (1994). Melt impregnation in mantle peridotites and cumulates from the Elba Island ophiolites, Italy. *Memorie della Societa Geologica Italiana*, *47*, 201–215.

Theye, T., Reinhardt, J., Goffe, B., Jolivet, L., & Brunet, C. (1997). Ferro-and magnesiocarpholite from the Monte Argentario (Italy): First evidence for high-pressure metamorphism of the metasedimentary Verrucano sequence, and significance for PT path reconstruction. *European Journal of Mineralogy*, *9*(4), 859–874. https://doi.org/10.1127/ejm/9/4/0859

Treves, B. (1984). Orogenic belts as accretionary prisms: The example of the northern Apennines. *Ofioliti*, *9*(3), 577–618.

Ujiie, K., & Kimura, G. (2014). Earthquake faulting in subduction zones: Insights from fault rocks in accretionary prisms. *Progress in Earth and Planetary Science*, *1*(1), 1–30. https://doi.org/10.1186/2197-4284-1-7

Ujiie, K., Yamaguchi, H., Sakaguchi, A., & Toh, S. (2007). Pseudotachylytes in an ancient accretionary complex and implications for melt lubrication during subduction zone earthquakes. *Journal of Structural Geology*, *29*(4), 599–613. https://doi.org/10.1016/j.jsg.2006.10.012

Vannucchi, P., & Bettelli, G. (2002). Mechanisms of subduction accretion as implied from the broken formations in the Apennines, Italy. *Geology*, *30*(9), 835–838. https://doi.org/10.1130/0091-7613(2002)030<0835:mosaai>2.0.co;2

Vannucchi, P., Remitti, F., & Bettelli, G. (2008). Geological record of fluid flow and seismogenesis along an erosive subducting plate boundary. *Nature*, *451*(7179), 699–703. https://doi.org/10.1038/nature06486

Vannucchi, P., Remitti, F., & Bettelli, G. (2012). Lateral variability of the erosive plate boundary in the Northern Apennines, Italy. *Italian Journal of Geosciences*, *131*(2), 215–227.

Vannucchi, P., Sage, F., Phipps Morgan, J., Remitti, F., & Collot, J. Y. (2012). Toward a dynamic concept of the subduction channel at erosive convergent margins with implications for interplate material transfer. *Geochemistry, Geophysics, Geosystems*, *13*(2). https://doi.org/10.1029/2011gc003846

Vignaroli, G., Faccenna, C., Jolivet, L., Piromallo, C., & Rossetti, F. (2008). Subduction polarity reversal at the junction between the Western Alps and the Northern Apennines, Italy. *Tectonophysics*, *450*(1–4), 34–50. https://doi.org/10.1016/j.tecto.2007.12.012

Viola, G., Torgersen, E., Mazzarini, F., Musumeci, G., van der Lelij, R., Schönenberger, J., & Garofalo, P. S. (2018). New constraints on the evolution of the inner Northern Apennines by K-Ar dating of Late Miocene-Early Pliocene compression on the Island of Elba, Italy. *Tectonics*, *37*(9), 3229–3243. https://doi.org/10.1029/2018tc005182

Viti, C., & Mellini, M. (1996). Vein antigorites from Elba Island, Italy. *European Journal of Mineralogy*, *8*(2), 423–434. https://doi.org/10.1127/ejm/8/2/0423

Viti, C., & Mellini, M. (1997). Contrasting chemical compositions in associated lizardite and chrysotile in veins from Elba, Italy. *European Journal of Mineralogy*, *9*(3), 585–596. https://doi.org/10.1127/ejm/9/3/0585

Viti, C., & Mellini, M. (1998). Mesh textures and bastites in the Elba retrograde serpentinites. *European Journal of Mineralogy*, *10*(6), 1341–1359. https://doi.org/10.1127/ejm/10/6/1341

Wakabayashi, J. (2019). Sedimentary compared to tectonically-deformed serpentinites and tectonic serpentinite mélanges at outcrop to petrographic scales: Unambiguous and disputed examples from California. *Gondwana Research*, *74*, 51–67. https://doi.org/10.1016/j.gr.2019.04.005

Zhang, J. (2020). The study of subduction channels: Progress, controversies, and challenges. *Science China Earth Sciences*, *63*(12), 1831–1851. https://doi.org/10.1007/s11430-019-9626-5

Zucchi, M. (2020). Faults controlling geothermal fluid flow in low permeability rock volumes: An example from the exhumed geothermal system of eastern Elba Island (northern Tyrrhenian Sea, Italy). *Geothermics*, *85*, 101765. https://doi.org/10.1016/j.geothermics.2019.101765